Running head: CONVEXITY OF THE UPPERMOST CONTINENTAL SLOPE

OCEANOGRAPHIC CURRENTS AND THE CONVEXITY OF THE UPPERMOST CONTINENTAL SLOPE

NEIL C. MITCHELL[1,*] AND JOHN M. HUTHNANCE[2]

[1]School of Earth, Ocean and Planetary Sciences, Cardiff University, Wales, UK

[2]Proudman Oceanographic Laboratory, Joseph Proudman building, 6 Brownlow Street, Liverpool L3 5DA, UK

*Now at: School of Earth, Atmospheric and Environmental Sciences, The University of Manchester, Williamson Building, Oxford Road, Manchester M13 9PL, UK.
Office: +44(0)161 2750779
School: +44(0)161 3069360
Fax: +44(0)161 3069361
Email: Neil.Mitchell@Manchester.ac.uk.

Keywords: continental shelf edge, bedload transport, continental slope morphology, sandy clinoforms, multibeam echosounder data.

ABSTRACT

Immediately below the shelf edge where sea-level lay during the Last Glacial Maximum (LGM), the uppermost continental slope in many areas has a smooth, convex-upwards rounded shape in profile. This shape is an example of a clinoform "rollover", a sedimentary feature that arises in general terms from how declining "energy" with water depth allows sediments to steepen. Computer models using the diffusion transport equation with mobility K declining with depth can produce rollover shapes, but the models have yet to be properly justified and the controls on K have been unclear. In this contribution, aspects of morphologic datasets from the USA and Iberian Atlantic margins are shown to be indeed compatible with the diffusion model. From experiments and theory, the gravity effect on saltating particles leads to a downslope flux that is proportional to local bed gradient, as required by the diffusion model, if the bed is agitated by oscillating currents of small residual current, by contour-parallel currents, or by a combination of both. The predicted mobility K is then an increasing function of the current's average speed. Near-bottom current-meter data reveal how currents, enhanced around the shelf edge, decline with water depth in a way that is generally compatible with the rollover morphology. During the LGM, bed currents due to tides and surface waves were stronger than at present. Although difficult to predict, they are expected to produce a more sharply declining mobility with depth that would be compatible with the limited depth range below the shelf edge over which sand and gravel have deposited.

1. INTRODUCTION

The shelf edge or break was defined originally in terms of the increase in gradient associated with it. For example, Heezen et al. (1959) mentioned that "The continental shelf ... extends from the shore line to the shelf break where the seaward gradient sharply increases to greater than 1:40." Although the shelf edge may have seemed abrupt with the vertical exaggeration typical of the older records from wide-beam echo sounders, in detail the bathymetry steepens gradually between shelf and slope (Bennett and Nelsen 1983; Field et al. 1983). In the higher-resolution bathymetry shown here, and in other datasets that we and others have studied (e.g., Adams and Schlager 2000), the uppermost slope from where sea level lay at ~ 120 m during the LGM down to a few hundred meters depth commonly has a convex form with gradually varying gradient. Where continental slopes have prograded, they form giant sigmoidal clinoforms, with this convex uppermost surface its "rollover" (Pirmez et al. 1998; Sangree and Widmier 1977).

Rollovers arise generally from a gradual variation in energy of the environment: in shallow water, strong currents due to tides and waves flatten sediment topography, whereas in deeper water, where currents are weaker, sediment can form steeper deposits. The analysis presented here is intended to contribute to developing a more quantitative basis for this general statement, using information from theory and experiments to suggest how bedload sediment should be mobilized by currents. Such models potentially allow variations in seabed morphology to be linked with variations of environment.

Although concerning mud rather than sand as here, previous modelling of rollovers illustrate the trade-off between energy and gradient. Friedrichs and Wright (2004) showed how shelf mud, when kept suspended by waves, can form a seaward-

travelling gravity flow that deposits as wave agitation decreases where the flow extends beyond surface influences. Their model deposits form rollovers typical of deltas found at muddy river mouths. In models for freshwater delta fronts (Bitzer and Harbaugh 1987; Pirmez et al. 1998), spreading and slowing of river outflow reduces bed shear stress, causing fine suspended sediment to deposit, over time also creating rollovers.

Diffusion transport models in which the mobility K declines with depth can also produce rollovers (Flemings and Grotzinger 1997; Kaufman et al. 1991; Rivenaes 1992; Rivenaes 1997; Schlager and Adams 2001; Syvitski and Daughney 1992). In our view, these models have not been well justified in marine settings because transport by many of the processes claimed to be represented by the models is inconsistent with the model's assumptions (Mitchell and Huthnance 2007). However, we show here how the effect of gravity on saltating sand could potentially lead to diffusion, suggesting a restricted application. By deriving the diffusion equation from first principles, a relationship of the mobility K to the speed of currents is found, thus allowing measurements of the modern currents to be compared via modelling with morphology, linking oceanographic environment to seabed evolution.

This paper is structured as follows. We first examine the logic behind the diffusion model. We then outline theory and experiments showing how the gravity effect on saltating particles does potentially lead to diffusion of seabed topography. A simple forward model illustrates how sandy rollovers could arise from the gravity effect. Using data from two sides of the Atlantic, we then describe and interpret observations of uppermost slope morphology that are consistent with the model, while also compiling data on modern bed currents to assess the extent to which currents intensify towards the shelf edge and contribute to the rollover form. The analysis then

examines how stronger, more sharply varying bottom currents during earlier times of lowered sea level provide a better explanation for how sand has deposited over a limited extent of the uppermost slope, interpreting the rollover form as a relic of LGM conditions.

THEORY

Diffusion Transport Models

In these models, a diffusion equation in surface topography H is used to represent how down-slope sediment transport processes tend to fill in basins over time (e.g., Driscoll and Karner 1999; Flemings and Grotzinger 1997; Granjeon and Joseph 1999; Jordan and Flemings 1991; Mitchell 1995; Mitchell 1996; Penn and Harbaugh 1999; Quiquerez et al. 2004; Wolfe et al. 1994). The equation often used is

$$\frac{\partial H}{\partial t} = K\nabla^2 H \quad (1),$$

where K is a mobility parameter (m^2/s). The Laplacian $\nabla^2 H$ represents the terrain's curvature. In these models, sediment accumulates in depressions because areas of positive $\nabla^2 H$ imply positive $\partial H/\partial t$ in equation (1). In the absence of other effects generating relief (e.g., channelled erosion or tectonics), the model topography becomes smooth over time.

The model originates in hillslope studies by combining an argument for how soils creep down-slope with an assumption that mass is locally conserved (Culling 1960; Culling 1963; Kirkby 1971). In linear creep (Small et al. 1999), soil moves at rates simply proportional to the local topographic gradient:

$$Q = -K\rho_s \, \partial H/\partial y \qquad (2)$$

where Q (kg/m/s) is the mass flux in the down-slope direction (y (m)) per unit width of

slope and ρ_s (kg/m^3) is the soil density. The continuity relation represents how a spatial change in soil flux implies erosion or deposition (conservation of mass):

$$\partial H/\partial t = -1/\rho_s \, \partial Q/\partial y \quad (3)$$

Differentiating Equation 2 in y and substituting in Equation 3 then leads to a diffusion equation in soil topography:

$$\frac{\partial H}{\partial t} = \frac{\partial}{\partial y}\left(K \frac{\partial H}{\partial y} \right) \quad (4a)$$

$$\text{or } \partial H/\partial t = K\partial^2 H/\partial y^2 \quad (4b)$$

if K is constant or varies gradually so that $\partial K/\partial y \cdot \partial H/\partial y << K\partial^2 H/\partial y^2$. Equation (1) can be derived by repeating this analysis in two dimensions.

If the model were to apply in marine settings, the sediment flux would need to occur in the down-slope direction and to have a magnitude proportional to the bed gradient (Equation 2). As outlined elsewhere (Mitchell and Huthnance 2007), the effects of many down-slope processes driven by gravity are unlikely to follow Equation 2 exactly, for example, slope failure and creep of clays involve threshold shear stresses so their fluxes are not simply proportional to gradient. Sedimentary flows possess momentum, so they are affected by upslope as well as local topography, and the processes by which they deposit sediment are complex. Fine-grained particles deposit at rates that are not necessarily related to bed gradient, but rather to bed shear stress (McCave and Swift 1976) and to factors stabilizing the surface against intermittently high stress (McCave 1984), so muddy clinoforms are better modelled using other schemes. The diffusion model therefore does not describe marine sediment transport generally, and its use should be limited to situations where its assumptions can be shown to be followed.

Gravity Effect on Saltating Particles

In as much as there is presently no general review of the gravity effect available, we summarize the literature in electronic supplement ES1 and reproduce key points here. Figure 1A shows a conceptual model for a fully developed bedload (Bagnold 1963), in which particles are mobile where the shear stress due to particle impacts with the bed exceeds a critical stress τ_0. The reaction to particle impacts effectively sets up a dispersive pressure which keeps particles water-borne. Ignoring initially the direct effect of the current, the force of gravity acting on particles then leads to a net stress on the mobile layer parallel to the bed causing down-slope movement that is stabilized by friction. According to this model, a greater thickness of particles (and greater flux) can be expected if the driving stress is larger because more particles will experience stresses above their critical value τ_0.

Generalizing this conceptual model to two dimensions to include both the direct current and gravity effects, the total bedload flux $\mathbf{Q_b}$ is:

$$\mathbf{Q_b} = S\,|\mathbf{u}|^2(\mathbf{u}-\lambda|\mathbf{u}|\nabla\mathbf{H})/g \qquad (5),$$

where S is a constant, $\lambda = 1/\tan\phi_s$, and $\nabla\mathbf{H}$ is bed gradient (bold symbols represent vectors, |...| the vector magnitude and $\tan\phi_s$ is the sediment friction coefficient) (Bailard and Inman 1981; Huthnance 1982a; Huthnance 1982b).

Of interest for morphological modelling, Equation 5 leads to sand flux simply proportional to bed gradient (and hence topographic diffusion similar to Equation 1) in two situations. First, where the current continually reverses, such as under surface waves, internal tides or topographic waves, Equation 5 is dominated by the term $\lambda|\mathbf{u}|\nabla\mathbf{H}$ if the vector average of $\mathbf{u}$ (i.e., the residual current) is small. Second, the current $\mathbf{u}$ is

commonly orthogonal to the gradient vector $\nabla \mathbf{H}$ (e.g., geostrophic residual currents flowing parallel to contours). Provided that the contour current is uniform along contours, the down-gradient component of $\mathbf{Q_b}$ is then proportional to the bed gradient and a diffusion equation can be constructed in the down-slope direction. Both of these situations are common near the shelf edge.

Although Bagnold's original approach has been criticized, in particular for weakly developed bedloads, these concepts help to visualize the origins of diffusion and why sediment mobility relates to current strength. The experimental results in Figure 2 reinforce this theory. In Figure 2A, bedload data collected using a longitudinal flume (Damgaard et al. 1997) show enhanced flux when flow was down-gradient and reduced flux when up-gradient, with almost a linear variation with gradient on average. The change in flux is relatively small for a small change in gradient (e.g., over 10˚) compared with the flux when the flume was horizontal, so the direct current effect (term in $\mathbf{u}$ in Equation 5) can easily dominate over the gravity effect (term in $\lambda|\mathbf{u}|\nabla \mathbf{H}$). The reason why the gravity effect can be effective in the oceans, leading to diffusion, however, is that many currents oscillate so that the direct effect cancels out. The results shown in Figure 2B (Damgaard et al. 2003) are complicated by a stronger current leading to suspension and bed rippling, but they nevertheless also show a gravity effect.

Sekine and Parker (1992) summarized models of bedload on slopes dipping transverse to the current (i.e., contour-following currents). They suggested the following equation for the ratio of down-gradient flux q_n to along-current flux q_s:

$$q_n/q_s = -B\,|\nabla \mathbf{H}|; \quad B = B_0(\tau_c/\tau_b)^m \qquad (6),$$

where B_0 and τ_b are constants and τ_c is the current shear stress. It also suggests a linear increase in the down-gradient flux with gradient $|\nabla \mathbf{H}|$ and that the flux increases with

the current strength. Sekine and Parker (1992) suggested that the main group of experimental data compiled in Figure 2C show that q_n is similarly or somewhat less rapidly varying with current stress than the q_s. Because the direct current flux q_s increases with u^3 or less (depending on importance of the threshold of motion) (Soulsby 1997), q_n is also proportional to u^3 or less. Based on all the information available (electronic supplement ES1), diffusion probably occurs with K proportional to between roughly u^2 and u^3, implying a strong sensitivity to bottom current strength.

Forward Simulation

A numerical model was used to illustrate how rollovers could persist as steady state features of depth-declining currents, if sea level, wave climate, ocean currents, and supplied sediment flux and texture were all steady. Only the gravity effect on bedload was accounted for. Although simple compared with natural systems, the simulations are intended to illustrate first-order controls, and the results are similar to those with sinusoidally varying water level (Kaufman et al. 1991).

In the model (Figure 3), sand was supplied at a constant flux Q_0 from the left boundary and its evolving surface was represented by an equally spaced array of elevation values, initially a simple ramp of gradient $\tan\gamma_0$. The variation of mean current speed $<|\mathbf{u}|>$ with depth d was approximated by a power law: $<|\mathbf{u}|> \propto d^{\beta}$ (which will be shown later to approximate currents on the USA Atlantic slope). The down-gradient flux of bedload was given by $Q_{by} \propto -<|\mathbf{u}|>^n \cdot \partial H/\partial y$, where $\partial H/\partial y$ is the offshore bed gradient and $n = 2$. Thus, $Q_{by} \propto -d^{2\beta}\partial H/\partial y$ was used to compute how the local flux varies with both current strength and bed gradient.

Bed gradients $\partial H/\partial y$ were derived from finite differences of the topography and elevations adjusted iteratively using the continuity relation ($\partial H/\partial t = -\partial Q_{by}/\partial y \cdot 1/\rho_s$). Because this scheme leads to sediment becoming infinitely mobile at sea level, a constant value for $d^{-2\beta}$ was imposed above a certain depth to maintain stability. (Coordinates are omitted from Figure 3 because we wish to emphasize how changes in parameters affect morphology but essentially the limiting depth for $d^{-2\beta}$ lies along the tops of the graphs.)

Figure 3A shows a simple developing clinoform, and the graph to its right shows bed gradients calculated from the final topography. In Figure 3B, the current speeds were varied more sharply with depth (double β), creating a markedly sharper rollover. With a doubling of Q_0 (Figure 3C), the rollover was also sharper. In Figure 3D, the ramp angle was doubled, producing a somewhat sharper rollover. The convexity of a sandy rollover therefore depends, not merely on the sharpness of the variation of currents with depth but also on the sediment input and, to a lesser degree, on the shape of the space in which the sediment accumulates.

The model rollover is only marginally below sea level, so the model does not predict the existence of a shelf. Clearly other processes generate shelves, such as subaerial erosion during sea-level lowstands. If gravity-driven bedload transport plays an important role, progradation of the uppermost slope occurs primarily during conditions of lowered sea level (with sea level intersecting the upper face of the rollover as in Figure 3) because extreme currents are needed in the shallow water to move the sediment on small gradients. Alternatively, if progradation is significant during high-stand conditions, other processes are needed to export sediment from the shelf.

These simulations represent sand only, but in practice mud depositing below the rollover (Chin et al. 1988; Deibert et al. 2003; Dunbar and Barrett 2005) forms a boundary condition to the gravity-driven transport of sand above. Mud depositing below the sand effectively elevates the clinoform face compared with its level if there were no mud available. Its long-term effect is therefore similar to the sand prograding over a shallower substrate, reducing convexity of the rollover.

Although the uncertainties in boundary conditions prevent subtle differences in rollover shapes from being interpreted, the observed rollover shape may reflect a particular pattern of currents. For example, the power-law depth-varying currents lead to steepening gradient-depth graphs, whereas a simulation developed using exponentially varying currents with depth (Figure 3E), such as might occur under waves with dominant height and period, has a flattening gradient-depth graph. As shown later, actual gradient trends are intermediate between these extremes.

3. MODERN CURRENTS

Near-bed measurements are compiled (Figure 4) to represent the average variation of bottom current speeds with depth (Figure 5). Data sources are given in electronic supplement ES2, which discusses measurement issues. The analysis mostly concerns USA Atlantic data collected over a year. Measurements were made at various altitudes but are left uncorrected because of insufficient information on bed roughness and boundary-layer development. The data in Figure 5 represent the effects of all current components including some oscillations under surface waves but primarily longer period oscillations, because surface waves have minor effect at depths of the continental slope and the meters tend to average out short period oscillations. The data

represent the average of the current speed, i.e., the scalar not the vector of current velocity.

3.1. *USA Atlantic*

Currents intensify up the USA slope towards the shelf edge, where they resuspend silt (Churchill et al. 1994). The dotted line in Figure 5A represents the average power-law trend of the near-bed data (solid symbols) below 150 m. The records for these sites show the different oceanographic influences, varying from long-period topographic Rossby waves (Gulf Stream eddy rings with 5 to 29 day periods) to high-frequency surface (wind) waves, with residual currents primarily along-slope (Aikman et al. 1988; Beardsley et al. 1985; Butman 1988; Butman et al. 1979; Csanady et al. 1988; Fratantoni et al. 2001; McClennen 1973; McGregor 1979; Shaw et al. 1994). Separating the data by frequency, Csanady et al. (1988) showed how the influence of the different oscillations varies: Rossy-wave currents affect the whole slope, whereas wind-driven upwelling or downwelling currents, tidal currents, and currents under surface waves are important over the upper slope but decline to 1000 m. Internal tides are enhanced near the shelf edge where a front between the shelf and slope water bodies intersects the seabed (Aikman et al. 1988; Flagg 1988; Ou and Maas 1988). Cacchione et al. (2002) showed how bed stresses from internal waves intensify where the bed gradient approaches the characteristic gradient of the waves, modulating how fine sediment deposits on the slope.

Somewhat different currents might be expected between sites, but comparisons between current meters suggests that, away from major canyons, the regression in Figure 5A approximates the typical uppermost slope enhancement. Figure 6 compares

the current variances computed by Csanady et al. (1988) for different frequency bands (see figure caption). The sites near 1000 m depth show a similar influence of Rossby waves. Higher-frequency currents in shelf-edge sites A and SF in Figure 4 are also comparable.

Iberia Atlantic

The fewer measurements made off Iberia are compiled in Figure 5B (electronic supplement ES2). The solid lines in Figure 5B show currents derived from 10 days of ship acoustic Doppler measurements (electronic supplement ES3; bold line is median average, and fine lines represent the inter-quartile range of current speed). The power-law trend (dotted line) was derived from all bottom-measured data below 150 m depth, including measurements from 100 m altitude above bottom to compensate for data scarcity. It suggests a more sharply varying speed with depth than off the USA. Although this difference is unresolved statistically, a sharp variation might be expected because of this area's exposure to Atlantic swell (Vitorino et al. 2002) and strong internal waves on the shelf (Jeans and Sherwin 2001; Sherwin et al. 2002; Vitorino et al. 2002).

Different wind directions in winter and summer lead to sustained downwelling and upwelling, respectively (Vitorino et al. 2002). On such easterly ocean margins, an equatorward wind stress induces an Ekman spiral (a Coriolis effect on the currents) and transport of surface water offshore relative to the water below. Upwelling of underlying water replaces surface water blown offshore. The sea surface is lowered at the coast, leading to an equatorward geostrophic current developing to balance the surface gradient, a current that is enhanced by the equatorward wind stress. Downwelling

occurs during the opposite conditions. Numerical models show that upwelling and downwelling lead to bed currents declining seawards from the shelf edge (Davies et al. 2002; Xing and Davies 2002), contributing to the trends observed in Figure 5B.

GEOLOGY AND MORPHOLOGICAL OBSERVATIONS

USA Atlantic Margin

Figure 7A shows bathymetry derived with continuous coverage of multibeam echo sounders. Above where the slope is incised by canyons, the topography is remarkably smooth and ridges between canyons are rounded rather than sharp. Figure 7B shows the median gradient (50%) and inter-quartile range of gradients (25% to 75%) for the area outlined in Figure 7A (where gradients were derived from differences in elevation in offshore and along-slope directions over a 50 m lengthscale after smoothing the bathymetry grid with a 250 m by 250 m filter (Wessel and Smith 1991)). Median gradient increases almost linearly with depth to 500 m, a variation implying that the morphology is exponential-like in profile, which is illustrated by the dashed exponential curves fitted by least-squares to the profiles shown in Figure 7C.

Figure 7B shows median grain sizes derived from grab sampling at sites located by solid star symbols in Figure 7A. Coinciding with the smooth morphology, the seabed is sandy at the surface, with a transition to mud at 300 m to 350 m. Published maps show this pattern of grading continuing along-strike (e.g., Keller et al. 1979; Southard and Stanley 1976; Stanley et al. 1983; Stanley and Wear 1978). Subsurface lithologies sampled at AMCOR 6007 drilled on the outer shelf (Figure 7A) include mostly sand of Pleistocene to Miocene age (Figure 7F) (Hathaway et al. 1979; Hathaway et al. 1976). From an ALVIN dive 50 km NE of Figure 7A, Malahoff et al.

(1982) noted an upwards change to coarser sand with pebbles, cobbles, and even some boulders above 380 m depth.

Two seismic reflection lines show a stratigraphic pattern typical of seaward progradation along with aggradation on the outer shelf. The multichannel data in Figure 7D, collected along the dashed line in Figure 7A (Schlee et al. 1976), show shallow-dipping foresets subparallel to the modern seabed. The single-channel data in Figure 7E also shows subparallel foresets but that the shelf edge stratigraphy overlies strata deeping shallowly seawards. Nevertheless, it confirms a lateral extension of the stratigraphy beneath the uppermost slope in Figure 7D, a pattern that is also mimicked in other seismic data collected nearby (McGregor et al. 1979; Schlee et al. 1979).

Iberian Atlantic Margin

Figure 8A shows bathymetry also collected with a multibeam echo sounder (NERC 2001). The morphology shallower than 500 m is smooth, similar to Figure 7A. Profiles "a" and "b" in Figure 8B also show a rounded shape. Median gradient (Figure 8C) of data from the area outlined in Figure 8A reveals a quasi-linear steepening with depth to 700 m, but with the rate of steepening only half that in Figure 7C. Multichannel seismic reflection data collected along the "Ewing" track shown in Figure 8A (Pérez Gussinyé 2000, her Figure 2.2) show reflectors beneath the outer shelf subparallel to the seabed to around 1 km sediment depth. Bottom photographs collected near 200 m depth (located by open circles in Figure 8A) show a bioturbated muddy sand (NERC 2001). Samples recovered near there and immediately shallower are fine-grained sands with < 25% silt and clay (mean grain size 2-3 ϕ) (Dias et al. 2002; Jouanneau et al. 2002; van Weering et al. 2002).

Interpretation of Morphology

Many of the topographic characteristics observed are typical of diffusion (Mitchell and Huthnance 2007). For example, the smoothness of the terrain is expected because, from Equation 1, bumps (negative $\nabla^2 H$) and depressions (positive $\nabla^2 H$) progressively attenuate (locations of negative and positive $\partial H/\partial t$, respectively) if not maintained by other effects. Furthermore, parabolic surfaces between canyon heads are also typical (though not necessarily diagnostic) of diffusion because the parabola is the steady state solution to the diffusion equation when material is removed constantly at the channels. Where the bed is sandy, we ascribe these observations to the gravity effect on saltating sand and true diffusion (Mitchell and Huthnance 2007).

The seismic data show that the morphology has prograded, so sand has been exported from the shelf persistently and spilled over the shelf edge. Spilled sand was mobilized by currents affecting the uppermost slope, leading to a gravity-driven movement of particles and a stratigraphic evolution similar to that illustrated in Figure 3.

In later analysis, we further assume that areas below present 150 m depth lay persistently below sea level during the LGM, based on work elsewhere (Yokoyama et al. 2000). A lack of significant glacio-isostasy in the area of Figure 7A is suggested by depths of submerged shorelines (Dillon and Oldale 1977), and a depth of 150 m keeps our analysis away from possible beach shoreface effects of the LGM.

DERIVING A MODEL *K* FROM MORPHOLOGY

We develop a kinematic model to invert the morphology for diffusion mobility K, which then allows us to compare the variation in the derived K with the currents, assuming that sediment mobility simply originates from the gravity effect on saltating particles. The results are not unique, so the exercise is intended rather to identify the range of values consistent with the model. An assumption of long-term steady state is required. In as much as seismic reflectors parallel the modern seafloor in these areas, the morphology is probably steady state over 100 ky to My timescales, depending on data resolution, but not necessarily so over shorter timescales.

Much of the following analysis is possible analytically because the uppermost slope is nearly exponential:

$$d' = d_0'\exp(sy) \qquad (7),$$

where $d' = d-d_r$ is depth below a reference depth d_r such that gradient $\partial H/\partial y = -sd'$ (i.e., linear with depth, Figure 2a), s is the rate of bed steepening with depth (herein called the convexity parameter) and y is distance offshore from where $d' = 0$. Parameters d_r = 111 and 136 m and s = 0.000679 and 0.000328 were obtained by least-squares regression of median gradient on depth from Figures 7B and 8B, respectively.

Deriving K_y Assuming that Sand Bypasses

If all sand exported from the shelf bypasses and none deposits, the offshore component of flux, $Q_{b,y}$, is then spatially uniform and K_y can be obtained simply by inverting Equation 1 (i.e., $K \propto 1/(|\nabla \mathbf{H}|)$). This is unrealistic, because sand has deposited over a restricted area beyond the outer shelf, but nevertheless the predicted variation in K_y shown in the first two graphs for K_y in Figure 9A (continuous lines "uniform Q") provides a limiting trend. (Here and in other graphs in Figure 9, values of K_y are shown

as both $K_y^{1/3}$ and $K_y^{1/2}$ to compare with the mean current speeds, assuming bedload models in which $Q_{by} \propto <|\mathbf{u}|>^3|\nabla \mathbf{H}|$ and $Q_{by} \propto <|\mathbf{u}|>^2|\nabla \mathbf{H}|$, respectively. Values were also normalized by dividing by the value for K_y at d' = 100 m.)

Deriving K_y for Prograding Geometries

Figure 10 shows the geometry used to calculate K_y more generally. This is done essentially by working out how average deposition rates have varied spatially and then deriving transport flux using the continuity relation. K is subsequently obtained from the flux and bed gradient (Equation 2).

If the uppermost slope aggrades uniformly, $\partial H/\partial t = A$ is uniform (Figure 10A). If instead the uppermost slope progrades (Figure 10B), deposition rates increase away from the outer shelf. Their values required to advance the morphology uniformly at rate $\partial y/\partial t$ (i.e., to maintain a steady state shape) are given by

$$\partial H/\partial t = -\partial d'/\partial y.\partial y/\partial t \quad (8)$$

If the rollover both aggrades and progrades (Figure 10C), A is added:

$$\partial H/\partial t = A-\partial d'/\partial y.\partial y/\partial t \quad (9a),$$

or $$\partial H/\partial t = A+sd'.\partial y/\partial t \quad (9b)$$

by replacing $\partial d'/\partial y$ with $-sd'$. We define a parameter $\tan\alpha = A/(\partial y/\partial t)$ representing the ratio of upwards to seawards growth of the rollover. Physically, α is the rollover's climbing angle, which in principle can be measured from seismic reflection data (Figure 10C). Replacing $\partial y/\partial t$ with $A/\tan\alpha$ then leads to

$$\frac{\partial H}{\partial t} = A\left(1+\frac{d's}{\tan\alpha}\right) \quad (10)$$

in which deposition rates increase linearly with depth change d'. (At larger scale, deposition rates decline down the continental slope (e.g., Sanford et al. 1990), but this is beyond the sandy area of interest.)

Equation 10 also shows that the convexity parameter s reflects how time-averaged deposition rates have varied. If the rollover is sharply convex (large s), sharply varying deposition rates are required to maintain the morphology.

Spatial variations in the time-averaged flux Q_y are derived by applying the continuity relation in y. Replacing $\partial H/\partial t$ of Equation 10 with $-1/\rho_s \partial Q_y/\partial y$ from Equation 3 and integrating in y produces

$$Q_y(y) = Q_{y0} - A\rho_s\left(y + \frac{d_0'}{\tan\alpha}\left(e^{sy} - 1\right)\right) \quad (11)$$

where Q_{y0} is the offshore component of flux on the outer shelf (at $y = y_0$ corresponding to where $d' = d_0'$). Replacing y using Equation 7 leads to

$$Q_y(d') = Q_{y0} - A\rho_s\left(\frac{\ln(d'/d_0')}{s} + \frac{(d' - d_0')}{\tan\alpha}\right) \quad (12).$$

If all flux Q_y occurs as gravity-driven bedload, K_y can be obtained from Equation 12. Because finer-grained material around the mudline is transported in suspension, obeying different transport rules, Equation 12 under-represents the sharpness of the true decline in sand Q_y with d'. Our interpretation therefore focuses on the upper part of the rollover.

K_y is derived from Equation 2, $\partial H/\partial y = -sd'$ and Equation 12 for Q_y:

$$K_y(d') = \frac{A\rho_s}{sd'}\left(\frac{Q_{y0}}{A\rho_s} - \frac{\ln(d'/d_0')}{s} - \frac{d' - d_0'}{\tan\alpha}\right) \quad (13)$$

The form of $K_y(d')$ thus depends on Q_{y0}, A, ρ_s, s, d_0', and α, of which s can be derived from bathymetry and α can in principle be estimated from seismic data. Although A,

Q_{y0}, and ρ_s could each be estimated separately if adequate stratigraphic and physical property data were available, we instead use their ratio $Q_{y0}/A\rho_s$ which is a lengthscale over which sediment of flux Q_{y0} would deposit at average rate A. d_0' was set to 1 m.

Comparing Inversion Results to Modern Current Data and LGM Conditions

Figures 9A and 9B show inversion results along with (dotted lines in graphs) the mean current speed variation from Figure 5A. Although the latter is only the mean, peak speeds (more relevant to mobilizing bedload) probably have a similar power-law trend, as suggested by the curves of Doppler data in Figure 5B in which the upper quartile parallels the median average. Threshold-of-motion effects should be considered in refinements of this model. From Figures 7D and 7E, the rollover climbing angle α is 11˚ to 16˚ (inversion results with α = 10˚ are most relevant, though others are shown to illustrate effect of uncertainty in α).

Figure 9B shows a relatively moderate decline in K with depth if the lengthscale $Q_{y0}/A\rho_s$ is large compared with the uppermost slope region of interest. The trend is somewhat steeper than the modern current data, although the difference may be less significant if thresholds of motion effects are considered (i.e., if the amount by which speed exceeds threshold decreases more greatly from 100 m to 300 m than the mean speed). There is little evidence that sand deposits over this lengthscale, however, based on the distance across the rollover to the sand/mud transition (Figure 7). More realistically, sand has deposited over a short distance of a few kilometers beyond the outer-shelf parts of the profiles in Figure 7C, so K_y must vary sharply with depth, as in Figure 9A, where trends are steeper than the current speed data.

Because much of the outer shelf sediment was deposited during the LGM (Southard and Stanley 1976), the uppermost slope morphology could reflect the stronger currents at that time. Although difficult to quantify, conditions during the LGM should have led to more sharply varying currents with depth than at present, consistent with the more steeply varying K_y. Bottom currents due to surface waves will have been more strongly felt with depressed sea level. Surface waves mobilizing sand to 200 m depth (Komar et al. 1972) could have affected the bed below present-day 300 m during the LGM. Figure 9C shows variations in peak bottom current speed u_s produced by 20 s and 10 s period storm waves with sea level depressed by 120 m (calculated with a deep-water approximation), which more closely match the inversion data in Figure 9A with $\alpha = 10^{\circ}$. Storms may also have been more frequent and vigorous based on enhanced NaCl and dust in ice cores (Mayewski et al. 1994).

It is difficult to say if other oceanographic currents would have had the same relation to the uppermost slope as in the modern data (Figure 5) because little is known about atmospheric forcing and ocean density stratification. Salinities of sediment pore waters suggest that the LGM oceans had a different density structure (Adkins et al. 2002), which could have affected internal-wave dynamics. An LGM tidal model (Egbert et al. 2004) suggests that M_2 tidal amplitudes were greater off the USA Atlantic coast by a factor of two, and may have been larger if the oceans were less density stratified than at present, e.g., because of lower surface temperature. Tidal flows at the shelf edge would have been further intensified because they supplied the high to low water volume via shallower depth over the outer shelf when sea level was lowered. Thus, although difficult to test formally, currents are expected to have been more

sharply varying with depth during the LGM, as we also suspect from the inversions of morphology and short deposition distance of the sand.

Effects of an Offshore Residual Current

If the residual (vectorally averaged) current has a finite component perpendicular to the shelf edge and it declines down the slope, an additional convergence of its associated sediment flux also contributes to prograding the uppermost slope (e.g., Quiquerez et al. 2004). Figure 11A shows such a decline in the mean offshore component of current-meter measurements from the two margins (Csanady et al. 1988; Huthnance et al. 2002).

A rough comparison with the gravity-driven offshore flux can be made using Equation 5. It suggests that the offshore current component dominates if $\langle u_y \rangle / \langle |\mathbf{u}| \rangle > |\nabla \mathbf{H}| / \tan\phi_s$. The dashed and dotted lines in Figure 11B show $|\nabla \mathbf{H}| / \tan\phi_s$ computed from the median gradients in Figures 7 and 8, respectively, and with $\tan\phi_s = 0.63$ (Soulsby 1997). A change from current-driven to gravity-driven transport with depth is suggested by the USA data values greater than $|\nabla \mathbf{H}| / \tan\phi_s$ at ~ 200 m but less than $|\nabla \mathbf{H}| / \tan\phi_s$ at 500 m. The Iberian values are both greater than $|\nabla \mathbf{H}| / \tan\phi_s$, however, suggesting that sand bedload transport is driven mainly by downwelling at present.

Diffusion in 2D

A diffusion equation with K declining with depth was applied to the bathymetry to explore tendencies of erosion or accumulation that would result if it were to apply universally above 300 to 350 m where sand exists. The calculation ignores how local

topography affects the currents, so only a general tendency implied by the variation of K with depth is sought, not one that applies exactly to all locations.

The bathymetry data (Figure 7A) were re-projected and smoothed with a 250 m filter. Local sand flux was calculated from $\mathbf{Q} = -K\nabla\mathbf{H}$, where gradient $\nabla\mathbf{H}$ (Figure 12A) was derived from finite differences of the bathymetry. The mobility was decreased inversely with depth d: $K = K_0(d/d_0)^{-1}$ where $d_0 = 1$ m is a reference depth. ($K \propto d^{-1}$ is nearly equivalent to using the trend in Figure 5A ($\beta = 0.36$) with $n = 3$.) Changes in topography were then calculated from continuity, $\partial H/\partial t = -\nabla.\mathbf{Q}$. The calculation was repeated iteratively, each time adjusting the bathymetry and re-calculating bed gradients to quantify $\mathbf{Q}$. The resulting depth change values are omitted from Figure 12B to highlight the pattern of relative change rather than absolute values, and results below 400 m are censored because the model is not relevant to the muddy slope sediments.

If Equation 1 were to apply uniformly with constant K, the spurs between canyon heads (areas of negative curvature) would erode (negative $\partial H/\partial t$) relative to the outermost shelf, where straight contours indicate smaller curvature. Figure 12B instead shows little bed change across the uppermost slope away from canyon heads because K decreasing sharply with depth compensates for increasing terrain curvature. Where the uppermost slope is sandy, therefore, the persistence of morphologic features of differing curvature may imply persistence in bottom current patterns too.

DISCUSSION

Previous studies reproducing clinoform rollovers with diffusion models (e.g., Flemings and Grotzinger 1997; Kaufman et al. 1991; Rivenaes 1997; Schlager and

Adams 2001) have, in our view, not adequately justified using the diffusion equation. From the justification using the gravity effect on saltating particles identified here, the bed shear stress or bottom current speed strongly control sediment mobility. It is probably not adequate to simulate the effects of sea-level fluctuations on transport by changing water depth alone (Flemings and Grotzinger 1997; Kaufman et al. 1991; Rivenaes 1997; Schlager and Adams 2001), because changing water depth also varies the tidal currents and because greater frequency of storms during the LGM implies a different influence of surface waves. The rounding of the shelf edge suggested as due to varying sea level or wave base level (Adams and Schlager 2000; Schlager and Adams 2001) is suggested here instead to reflect the way in which bed shear stress varies with depth, a more gradually curved rollover arising from gradually varying shear stress with depth. Furthermore, sharp rollovers have been produced with models in which K is constant in the water column and interpreted as representing a lack of near-surface influences (Schlager and Adams 2001). In such models, however, an abruptly increased K above the water line is often used to simulate high mobility of sediment where exposed subaerially, so such models should prompt us to consider whether sharp rollovers in data imply abruptly varying K, not necessarily a lack of near-surface influences.

The sensitivity of K to current speeds has implications for interpreting relative sea-level change from margin sequences (Vail et al. 1977). Flemings and Grotzinger (1997) illustrated how fluctuations in sediment supply can generate sequences of character similar to those generated by sea-level fluctuations (Christie-Blick and Driscoll 1995). If the enhanced salt concentrations in ice cores (Mayewski et al. 1994) implies an enhanced storm frequency and/or severity, the mean bed current speed in

wave-dominated environments should be enhanced, implying an increase in mobility K. For example, a doubling of storm frequency would imply doubling of $<|\mathbf{u}|>$, increasing K by a factor 4 to 8 (from $K \propto <|\mathbf{u}|^2>$ to $K \propto <|\mathbf{u}|^3>$). Combined with varying residual currents, variations in "oceanic climate" can potentially affect unconformities and obscure simple effects of sea-level fluctuation on sequences, which are often guided by geometry of strata around the rollover (Steckler et al. 1999).

Although the single-component model developed here usefully provides insights, it lacks many effects which need further investigation before incorporating them into more complete models (e.g., Quiquerez et al. 2004). To include bedload transport by residual currents, we would need to predict upwelling or downwelling currents of earlier periods when less information on wind conditions are available. How mud components within the rollover and below it contribute to rollover convexity are difficult to address because of difficulty in predicting biological and physical stabilisation under time-varying currents (McCave 1984; Sanford and Maa 2001).

The activity of fish and other organisms can also affect seabed morphology over geological periods, and the gravity effect on biologically resuspended particles potentially contributes to topographic diffusion (Mitchell and Huthnance 2007). Because lateral sediment fluxes from by biological activity have not been quantified, its morphological effect is difficult to assess quantitatively, but bio-mixing rates of radiometric tracers in cores typically decline below the shelf edge mimicking the decline in current speeds (Anderson et al. 1988; Henderson et al. 1999; Middelburg et al. 1997; Schmidt et al. 2002; Soetaert et al. 1996).

Examining the geometry of older strata can potentially inform this problem because transport consistent with a diffusion-type model implies that strata should

steepen if sediment flux increases (Schlager and Adams 2001). This can be seen from Equation 2: $\partial H/\partial y$ increases if K and ρ are constant but Q increases. Alternatively, if Q were constant but there were a change in oceanographic conditions, then K could vary and also affect the steepness of strata.

In some seismic datasets, the ancient rollover is more rounded than the modern rollover, possibly reflecting effects of K and Q. This can be seen, for example, in data collected across the shelf edge in the South Western Approaches to the UK and France, where Pleistocene sediments have a markedly sharper rollover than their underlying upper Miocene (Bourillet et al. 2003), which largely comprises sand (Evans and Hughes 1984; Pantin and Evans 1984). The modern surface is consistent with diffusion (Mitchell and Huthnance 2007), being smooth aside from bedform relief (Cunningham et al. 2005).

A similar sharpening, from Late Oligocene towards Pleistocene, can be seen in the New Jersey shelf edge of Steckler et al. (1999). Their reconstructions suggest that the uppermost slope was more gradually curved (e.g., $s' = 2 \times 10^{-4}$ m^{-1} for their m6 surface) than we find for the area in Figure 7 ($s' = 6.74 \times 10^{-4}$ m^{-1}). Evidence that bedload transport and hence the gravity effect was involved in creating these rollovers includes rounding of grains sampled in the Miocene strata (Poppe et al. 1990).

These two examples could potentially reflect changes in oceanographic conditions. The Miocene and earlier periods were times of more stable sea level with variations of < 50 m (John et al. 2004; Kominz et al. 1998; Kominz and Pekar 2001; Miller et al. 1998; Van Sickel et al. 2004) and extreme low-stands rarely reaching 100 m based on foraminiferal $\delta^{18}O$ (John et al. 2004; Lear et al. 2004). The enhanced tidal currents and oscillating currents due to storm-induced waves for the LGM shelf edge

should therefore have been less frequent during these previous periods compared with the Pleistocene. Thus, before the Pleistocene, more stable conditions imply long periods with a more gradually varying mobility with depth, in turn leading to a more gradually curved uppermost slope.

Sediment fluxes to the margins also generally increased into the Pleistocene associated with enhanced continental erosion of the glacial world, potentially leading to sharpened rollovers of sand. Enhanced fluxes are suggested, for example, by deposition rates in marginal basins dramatically increasing globally during the last 2 to 4 Ma [Zhang, 2001 #2454]. Furthermore, in Steckler et al.'s (1999) reconstructions, the shelf edge is sharper in the Middle Miocene than in the Late Oligocene, tracking an increased rate of sediment supply implied by the margin progradation rate.

CONCLUSIONS

The morphology of the uppermost slope is consistent with having been modified as though by a diffusion equation with mobility K declining with depth, generating the rollover and smooth, parabolic regions between canyon heads. Given the presence of sand and how modern currents decline with depth, the gravity effect on saltating particles provides a plausible explanation for this apparent diffusion. The sand has deposited relatively close to the outermost shelf, which implies that mobility declines sharply with depth. This could be consistent with stronger currents that declined more rapidly with depth during the Last Glacial Maximum. The models imply that both the sharpness of the uppermost slope rollover in profile and morphology in plan view depend on how the currents vary spatially, as well as on sediment flux to the slope and accommodation space.

Acknowledgments This work is based on multibeam sonar and geological data made freely available by the NOAA. The Iberian (OMEX-II) data were collected with funding from the European Union. John Humphrey (Proudman Laboratory) compiled the OMEX-II seabed photographs mentioned. Rose Anne Weissel (Lamont-Doherty) helpfully scanned the Robert Conrad seismic data for us. Rui Quartau provided some bathymetry data from the Iberian margin. We acknowledge discussions with Alan Davies and Jiuxing Xing, and a review of an earlier version of this paper by R. Larter. This paper was significantly improved thanks to helpful comments from Erwin Adams, Greg Fulthorpe, Colin North, and an anonymous reviewer. Figures were created with the "GMT" software system (Wessel and Smith 1991). JMH was supported by the Natural Environment Research Council and NCM was supported by a University Research Fellowship from the Royal Society during part of this work.

Figure captions

Figure 1. A) Illustration of particle motions in a bedload active on a slope. The long-dash line separates the bedload from the immobile bed below, defined as the level at which shear stresses equal the threshold of motion. B) Down-gradient movement arises because the momentum transfer from grain to grain collisions keeping the bedload mobile acts perpendicular to the bed on average ("dispersive pressure"), whereas the bedload weight acts vertically, leading to a net pressure acting parallel to the bed (gray vector) which becomes balanced by friction. Current shear stress components are omitted.

Figure 2. A) Measurements of sediment flux Q as a function of longitudinal gradient for experiments (Damgaard et al. 1997) with the bed Shields stress θ values shown. Enlarged symbols represent average Q for given gradient groupings (plus and gray-filled symbols only). The oblique lines are least-squares regressions of Q on gradient for the different stresses excluding data for -29°, which show enhanced Q near the sediment angle of repose. B) Experiments similar to Part A made at higher flow stress and with flux measured using a sediment trap (plus symbols) and with instruments designed to measure suspended particle flux (gray-filled circles). Bold plus symbols represent average Q calculated for groups of gradient. Dashed line is least-squares regression of the trap fluxes. C) Measurements of transverse bed-load flux against bed shear stress (Sekine and Parker 1992). Plus symbols: data collected in air (Yamasaka et al. 1987). Solid circles: data collected in water (Hasegawa 1981). Dashed lines represent graph trends expected with m of Equation ES10 equal to the values shown.

Figure 3. Results of numerical models exploring the effect of parameters on the shape of a sandy clinoform, assuming that sediment movements occur only because of the gravity effect on saltating particles. Initial bed topography is a simple ramp of gradient $\tan\gamma_0$ and sand is supplied from the left boundary with constant flux. Graph A is the reference model and B, C and D show the effects of varying the gradient of current speed with depth, input flux and ramp angle, respectively. Graphs to right show the final bed gradient versus depth (gradients in Part B are reduced by a factor of 20). The convexity s values shown were derived by least-squares regression of the gradients with depth over the depth intervals above the dashed lines. Lowermost graph was produced with current speeds varying exponentially with depth.

Figure 4. Locations of the study areas in Figures 7 and 8 (gray-filled boxes) and current-meter deployments. Gray depth contours shown annotated in kilometers were derived from Smith and Sandwell (1997). Black contour represents 200 m depth, marking the shelf edge. For the USA side, symbols represent data reported by (solid squares) Csanady et al. (1988) and (solid diamonds) Butman (1988). Plus symbols represent further data collected above 150 m depth, included for completeness (Butman 1988; Butman et al. 1979; Csanady et al. 1988; McClennen 1973). Open squares and diamonds represent data (Csanady et al. 1988; Butman et al. 1988) collected at altitudes above bottom of 100 m and ~ 50 m, respectively. Current meters at sites 5, F, A, and SF provided the data in Figure 6. Black star next to "Fig 2" locates the AMCOR 6007 well (Hathaway et al. 1976). For the Iberian margin, symbols represent data reported by (solid squares) Huthnance et al. (2002) and (solid circles) Thomsen et al. (2002), and other data collected during (star symbols) the WOCE and (solid diamonds) OMEX-II experiments (details in electronic supplement ES2). Fine solid line is path of measurements with a hull-mounted Doppler current profiler used to derive the trends in Figure 5B (electronic supplement ES3).

Figure 5. Mean values of current speeds measured with bottom-moored current meters, from the sources given in electronic supplement ES2 and at the locations in Figure 4 (identified with corresponding symbols). Data are shown at the local water depth of the mooring rather than instrument depth (heights above bottom are given in electronic supplement ES2). Dotted lines show trend of $\log_{10}\langle|\mathbf{u}|\rangle$ versus $\log_{10}d$ obtained from data below 150 m depth by least squares. Lines in Part B are median (bold, 50%) and

inter-quartile range (fine lines, 25%, 75%) of further near-bed current speeds derived from a hull-mounted acoustic Doppler current profiler (electronic supplement ES3).

Figure 6. Comparison of current variance at different locations along the USA margin. Variance was derived (Csanady et al. 1988) by multiplying power spectral density of current velocity by the width of each period bands. Period bands are 5.4 to 29.3 days (T, topographic waves), 30 h to 5.4 days (WD, wind-driven), 15.2 to 30 h (I/D, intertial-diurnal), 10.6 to 15.1 h (SD, semidiurnal), and < 10.6 h (HF, high frequency). A) Comparison of slope sites (solid symbols) MASAR-F and (open symbols) SEEP-I site 5. B) Comparison of shelf-edge sites (solid symbols) NASACS-SF and (open symbols) MASAR-A. Sites are located in Figure 4.

Figure 7. A) Map of the uppermost slope off the central Atlantic USA derived from continuous multibeam sonar data (National Geophysical Data Center Coastal Relief Model, www.ngdc.noaa.gov). B) Median and inter-quartile range of seabed gradient $|\nabla \mathbf{H}|$ and median grain size versus depth. Gradients were calculated from the data outlined in Part A. Grain sizes were measured by NOAA scientists from grab samples collected at sites located by solid star symbols in Part A. C) Sections across the uppermost slope between the diamond symbols in Part A, along with (dashed curves) Equation 7 fitted to the topography by least squares. D) Multichannel seismic section (Schlee et al. 1976; Schlee et al. 1979). E) Single channel seismic section collected along the continuous line in Part A by Lamont-Doherty scientists. F) Summary of sediments recovered at well AMCOR 6021 (Hathaway et al. 1976) with gray-scale

representing (white) sand, (light gray) silty and clayey sand, (mid-gray) silty clay, and (dark gray) clay. Vertical solid bar marks the vertical extent of the well.

Figure 8. A) Bathymetry of the Iberian Atlantic upper slope derived from multibeam echo-sounder data (NERC 2001). Solid line is the path of a multichannel seismic section (Pérez Gussinyé 2000, her Figure 2.2). Open circles mark bottom-photograph sites (NERC 2001). Two open star symbols mark sites of bottom-current measurements (Huthnance et al. 2002). B) Sections through the lines "a" and "b" marked Part A. C) Median (bold) and inter-quartile range of bed gradient calculated for the area outlined in Part A.

Figure 9. Variation of K with depth derived from the morphology. To compare with the current data, each pair of graphs shows the variation in $K^{1/3}$ and $K^{1/2}$, corresponding to bedload models in which $Q_{by} \propto <|\mathbf{u}|>^3|\nabla \mathbf{H}|$ and $Q_{by} \propto <|\mathbf{u}|>^2|\nabla \mathbf{H}|$, respectively. Dotted line is the regression of Figure 5A for comparison. A) K varies sharply with depth if sediment has deposited over a short lengthscale, implying a more sharply varying current speed with depth than presently observed. Also shown are curves assuming the sediment simply bypasses (uniform Q assumption). B) K varies more slowly with depth if the sediment deposits over a (probably unrealistic) longer lengthscale. C) Peak speed of bottom currents produced by extreme surface waves with the amplitudes and periods shown and with sea level 120 m lower than present (deep-water approximation).

Figure 10. Geometrical relationships for deriving the pattern of deposition rate required to maintain the rollover as a steady-state feature. A) The rollover grows vertically by aggrading uniformly at rate A. B) The rollover progrades at a uniform rate dy/dt. C) The rollover both aggrades and progrades, climbing at angle α.

Figure 11. A) The mean offshore current velocity of (solid circles) Csanady et al. (1988) for the USA sites and (solid stars) Huthnance et al. (2002) for the two Iberian sites (Figure 8A). The two open circles represent Csanady et al.'s data from their sites A and F located in Figure 4. B) The ratio of the mean offshore velocity to mean speed. All near-bottom data are shown, including those collected 100 m above bottom. Depths represent local water depths of measurements. Dashed and dotted lines represent thresholds between current- and gravity-dominated transport for the USA and Iberia areas, respectively (see main text for explanation).

Figure 12. A) Bed gradient in degrees calculated from the USA bathymetry (Figure 7). Contours are annotated in meters. B) Relative changes in bed topography predicted with the diffusion model with mobility K decreasing with depth. Data below 400 m have been censored, because the model does not apply to the slope muds. Note lack of change on spurs between canyon heads.

REFERENCES

ADAMS, E.W., and SCHLAGER, W., 2000, Basic types of submarine slope curvature: Journal of Sedimentary Research, v. 70, p. 814-828.

ADKINS, J.F., MCINTYRE, K., and SCHRAG, D.P., 2002, The salinity, temperature, and $\delta^{18}O$ of the glacial deep ocean: Science, v. 298, p. 1769-1773.

AIKMAN, F., OU, H.W., and HOUGHTON, R.W., 1988, Current variability across the New England continental shelf-break and slope: Continental Shelf Research, v. 8, p. 625-651.

ANDERSON, R.F., BOPP, R.F., BUESSELER, K.O., and BISCAYE, P.E., 1988, Mixing of particles and organic constituents in sediments from the continental shelf and slope off Cape Cod: SEEP-I results: Continental Shelf Research, v. 8, p. 925-946.

BAGNOLD, R.A., 1963, Mechanics of marine sedimentation, *in* Hill, M.N., ed., The Sea, vol. 3: New York, Wiley, p. 507-528.

BAILARD, J.A., and INMAN, D.L., 1981, An energetics bedload model for a plane sloping beach: local transport: Journal of Geophysical Research, v. 86, p. 2035-2043.

BEARDSLEY, R.C., CHAPMAN, D.C., BRINK, K.H., RAMP, S.R., and SCHLITZ, R., 1985, The Nantucket Shoals Flux Experiment (NSFE79). Part I: a basic description of the current and temperature variability: Journal of Physical Oceanography, v. 15, p. 713-748.

BENNETT, R.H., and NELSEN, T.A., 1983, Seafloor characteristics and dynamics affecting geotechnical properties at shelfbreaks, *in* Stanley, D.J., and Moore, G.T., eds., The Shelfbreak: Critical Interface on Continental Margins: Tulsa, Oklahoma, Society of Economic Paleontologists and mineralogists, p. 333-355.

BITZER, K., and HARBAUGH, J.W., 1987, DEPOSIM: a Macintosh computer model for two-dimensional simulation of transport, deposition and erosion, and compaction of clastic sediments: Computers & Geosciences, v. 13, p. 611-637.

BOURILLET, J.-F., REYNAULD, J.-Y., BALTZER, A., and ZARAGOSI, S., 2003, The 'Fleuve Manche': the submarine sedimentary features from the outer shelf to the deep-sea fans: Journal of Quaternary Sciences, v. 18, p. 261-282.

BUTMAN, B., 1988, Downslope Eulerian mean flow associated with high-frequency current fluctuations observed on the outer continental shelf and upper slope along the north-eastern United States continental margin: Implications for sediment transport: Continental Shelf Research, v. 8, p. 811-840.

BUTMAN, B., NOBLE, M., and FOLGER, D.W., 1979, Long-term observations of bottom current and bottom sediment movement on the mid-Atlantic continental shelf: Journal of Geophysical Research, v. 84, p. 1187-1205.

CACCHIONE, D.A., PRATSON, L.F., and OGSTON, A.S., 2002, The shaping of continental slopes by internal tides: Science, v. 296, p. 724-727.

CHIN, J.L., CLIFTON, H.E., and MULLINS, H.T., 1988, Seismic stratigraphy and late Quaternary shelf history, south-central Monterey Bay, California: Marine Geology, v. 81, p. 137-157.

CHRISTIE-BLICK, N., and DRISCOLL, N.W., 1995, Sequence stratigraphy: Annual Reviews of Earth and Planetary Sciences, v. 23, p. 451-478.

CHURCHILL, J.H., WIRICK, C.D., FLAGG, C.N., and PIETRAFESA, L.J., 1994, Sediment resuspension over the continental shelf east of the Delmarva Peninsula: Deep-Sea Research II, v. 41, p. 341-363.

CSANADY, G.T., CHURCHILL, J.H., and BUTMAN, B., 1988, Near-bottom currents over the continental slope in the Mid-Atlantic Bight: Continental Shelf Research, v. 8, p. 653-671.

CULLING, W.E.H., 1960, Analytical theory of erosion: Journal of Geology, v. 68, p. 336-344.

CULLING, W.E.H., 1963, Soil creep and the development of hillside slopes: Journal of Geology, v. 71, p. 127-161.

CUNNINGHAM, M.J., HODGSON, S., MASSON, D.G., and PARSON, L.M., 2005, An evaluation of along- and down-slope sediment transport processes between Goban Spur and Brenot Spur on the Celtic Margin of the Bay of Biscay: Sedimentary Geology, v. 179, 99-116.

DAMGAARD, J., SOULSBY, R., PEET, A., and WRIGHT, S., 2003, Sand transport on steeply sloping plane and ripple beds: Journal of Hydraulic Engineering, v. 129, p. 706-719 , DOI: 10.1061/(ASCE)0733-9429(2003)129.:9(706).

DAMGAARD, J.S., WHITEHOUSE, R.J.S., and SOULSBY, R.L., 1997, Bed-load sediment transport on steep longitudinal slopes: Journal of Hydraulic Engineering, v. 123, p. 1130-1138.

DAVIES, A.M., XING, J., HUTHNANCE, J.M., HALL, P., and THOMSEN, L., 2002, Models of near-bed dynamics and sediment movement at the Iberian margin: Progress in Oceanography, v. 52, p. 373-397.

DEIBERT, J.E., BENDA, T., LOSETH, T., SCHELLPEPER, M., and STEEL, R.J., 2003, Eocene clinoform growth in front of a storm-wave-dominated shelf, Central Basin, Spitsbergen: no significant sand delivery to deepwater areas: Journal of Sedimentary Research, v. 73, p. 546-558.

DIAS, J.M.A., GONZALEZ, R., GARCIA, C., and DIAZ-DEL-RIO, V., 2002, Sediment distribution patterns on the Galicia-Minho continental shelf: Progress in Oceanography, v. 52, p. 215-231.

DILLON, W.P., and OLDALE, R.N., 1977, Late Quaternary sea-level curve: reinterpretation based on glaciotectonic influence: Geology, v. 6, p. 56-60.

DRISCOLL, N.W., and KARNER, G.D., 1999, Three-dimensional quantitative modeling of clinoform development: Marine Geology, v. 154, p. 383-398.

DUNBAR, G.B., and BARRETT, P.J., 2005, Estimating palaeobathymetry of wave-graded continental shelves from sediment texture: Sedimentology, v. 52, p. 253-269.

EGBERT, G.D., RAY, R.D., and BILLS, B.G., 2004, Numerical modeling of the global semidiurnal tide in the present day and in the last glacial maximum: Journal of Geophysical Research, v. 109, Art. No. C03003.

EVANS, C.D.R., and HUGHES, M.J., 1984, The Neogene succession of the South Western Approaches, Great Britain: Geological Society of London Journal, v. 141, p. 315-326.

FERNANDEZ LUQUE, R., and VAN BEEK, R., 1976, Erosion and transport of bed load sediment: Journal of Hydraulics Research, v. 14, p. 127-144.

FIELD, M.E., CARLSON, P.R., and HALL, R.K., 1983, Seismic facies of shelfedge deposits, U. S. Pacific continental margin, *in* Stanley, D.J., and Moore, G.T., eds., The Shelfbreak: Critical Interface on Continental Margins: Tulsa, Oklahoma, Society of Economic Paleontologists and Mineralogists, p. 299-313.

FLAGG, C.N., 1988, Internal waves and mixing along the New England shelf-slope front: Continental Shelf Research, v. 8, p. 737-756.

FLEMINGS, P.B., and GROTZINGER, J.P., 1997, STRATA: freeware for analysing clastic stratigraphic problems: GSA Today, v. 6(12), p. 1-7.

FRATANTONI, P.S., PICKART, R.S., TORRES, D.J., and SCOTTI, A., 2001, Mean structure and dynamics of the shelfbreak jet in the Middle Atlantic Bight during fall and winter: Journal of Physical Oceanography, v. 31, p. 2135-2156.

FRIEDRICHS, C.T., and WRIGHT, L.D., 2004, Gravity-driven sediment transport on the continental shelf: implications for equilibrium profiles near river mouths: Coastal Engineering, v. 51, p. 795-811.

GRANJEON, D., and JOSEPH, P., 1999, Concepts and applications of a 3-D multiple lithology diffusive model in stratigraphic modeling, *in* Numerical Experiments in Stratigraphy: Recent Advances in Stratigraphic and Sedimentologic Computer Simulations, eds., *J. W. Harbaugh, W. L. Watney, E. Rankey, R. Slingerland, R. Goldstein, and E. Franseen*: SEPM, Special Publication 62, p. 197-210.

HASEGAWA, K., 1981, Bank-erosion discharge based on a non-equilibrium theory: Japanese Society of Civil Engineering Transactions, v. 316, p. 37-52 (in Japanese).

HATHAWAY, J.C., POAG, C.W., VALENTINE, P.C., MILLER, R.E., SCHULTZ, D.M., MANHEIM, F.T., KOHOUT, F.A., BOTHNER, M.H., and SANGREY, D.A., 1979, U.S. Geological Survey core drilling on the Atlantic shelf: Science, v. 206, p. 515-527.

HATHAWAY, J.C., SCHLEE, J.S., POAG, C.W., VALENTINE, P.C., WEED, E.G.A., BOTHNER, M.H., KOHOUT, F.A., MANHEIM, F.T., SCHOEN, R., MILLER, R.E., and SCHULTZ, D.M., 1976, Preliminary summary of the 1976 Atlantic margin coring project of the U. S. Geological Survey: U.S. Geological Survey Open-File Report 76-844, p. 220.

HEEZEN, B.C., THARP, M., and EWING, M., 1959, The floors of the oceans: 1. The North Atlantic: New York, The Geological Society of America, Special Paper 65, 122 p.

HENDERSON, G.M., LINDSAY, F.N., and SLOWEY, N.C., 1999, Variation in bioturbation with water depth on marine slopes: a study of the Little Bahamas Bank: Marine Geology, v. 160, p. 105-118.

HUTHNANCE, J.M., 1982a, On one mechanism forming linear sand banks: Estuarine, Coastal and Shelf Science, v. 14, p. 79-99.

HUTHNANCE, J.M., 1982b, On the formation of sand banks of finite extent: Estuarine, Coastal and Shelf Science, v. 15, p. 277-299.

HUTHNANCE, J.M., HUMPHERY, J.D., KNIGHT, P.J., CHATWIN, P.G., THOMSEN, L., and WHITE, M., 2002, Near-bed turbulence measurements, stress estimates and sediment mobility at the continental shelf edge: Progress in Oceanography, v. 52, p. 171-194.

JEANS, D.R.G., and SHERWIN, T.J., 2001, The evolution and energetics of large amplitude nonlinear internal waves on the Portuguese shelf: Journal of Marine Research, v. 59, p. 327-353.

JOHN, C.M., KARNER, G.D., and MUTTI, M., 2004, $\delta^{18}O$ and Marion Plateau backstripping: Combining two approaches to constrain late middle Miocene eustatic amplitude: Geology, v. 32, p. 829-832.

JORDAN, T.E., and FLEMINGS, P.B., 1991, Large-scale stratigraphic architecture, eustatic variation, and unsteady tectonism: a theoretical evaluation: Journal of Geophysical Research, v. 96, p. 6681-6699.

JOUANNEAU, J.M., WEBER, O., DRAGO, T., RODRIGUES, A., OLIVEIRA, A., DIAS, J.M.A., GARCIA, C., SCHMIDT, S., and REYSS, J.L., 2002, Recent sedimentation and sedimentary budgets on the western Iberian shelf: Progress in Oceanography, v. 52, p. 261-275.

KAUFMAN, P., GROTZINGER, J.P., and MCCORMICK, D.S., 1991, Depth-dependent

diffusion algorithm for simulation of sedimentation in shallow marine depositional systems, *in* Sedimentary Modeling: Computer Simulations and Methods for Improved Parameter Definition, eds. *E. K. Franseen, W. L. Watney, C. G. St. C. Kendall, and W. Ross*, Kansas Geological Survey, Special Publication Bulletin 233.

KELLER, G.H., LAMBERT, D.N., and BENNETT, R.H., 1979, Geotechnical properties of continental slope deposits- Cape Hatteras to Hydrographer Canyon, in Geology of Continental Slopes, eds L. J. Doyle and O. H. Pilkey, SEPM Special Publication 27, p. 131-153.

KIRKBY, M.J., 1971, Hillslope process - response models based on the continuity equation: Institute of British Geographers, Transactions, Special Publication 3, p. 15-30.

KOMAR, P.D., NEUDECK, R.H., and KULM, L.D., 1972, Observations and significance of deep-water oscillatory ripple marks on the Oregon contental shelf, *in* Swift, D.J.P., Duane, D.B., and Pilkey, O.H., eds., Shelf Sediment Transport: Processes and Pattern: Stoudsburg, Pennsylvania, Dowden, Hutchinson & Ross, p. 601-609.

KOMINZ, M.A., MILLER, K.G., and BROWNING, J.V., 1998, Long-term and short-term global Cenozoic sea-level estimates: Geology, v. 26, p. 311-314.

KOMINZ, M.A., and PEKAR, S.F., 2001, Oligocene eustasy from two-dimensional sequence stratigraphic backstripping: Geological Society of America, Bulletin, v. 113, p. 291-304.

LEAR, C.H., ROSENTHAL, Y., COXALL, H.K., and WILSON, P.A., 2004, Late Eocene to early Miocene ice sheet dynamics and the global carbon cycle: Paleoceanography, v. 19, p. PA4015; doi:10.1029/2004PA001039.

MALAHOFF, A., EMBLEY, R.W., and FORNARI, D.J., 1982, Geomorphology of Norfolk and Washington Canyons and the surrounding continental slope and upper rise as observed with DSRV Alvin, *in* Scrutton, R.A., and Talwani, M., eds., The Ocean Floor: New York, John Wiley & Sons, p. 97-111.

MAYEWSKI, P.A., MEEKER, L.D., WHITLOW, S., TICKLER, M.S., MORRISON, M.C., BLOOMFIELD, P., BOND, G.C., ALLEY, R.B., GOW, A.J., GROOTES, P.M., MEESE, D.A., RAM, M., TAYLOR, K.C., and WUMKES, W., 1994, Changes in atmospheric circulation and ocean ice cover over the North Atlantic during the last 41,000 years: Science, v. 263, p. 1747-1751.

MCCAVE, I.N., 1984, Erosion, transport and deposition of fine-grained marine sediments, *in* Stow, D.A.V., and Piper, D.J.W., eds., Fine-Grained Sediments: Deep Water Processes and Facies: Oxford, U.K., Blackwell Scientific, p. 35-69.

MCCAVE, I.N., and SWIFT, S.A., 1976, A physical model for the rate of deposition of fine-grained sediments in the deep sea: Geological Society of America, Bulletin, v. 87, p. 541-546.

MCCLENNEN, C.E., 1973, New Jersey continental shelf near bottom current meter records and recent sediment activity: Journal of Sedimentary Petrology, v. 43, p. 371-380.

MCGREGOR, B.A., 1979, Current meter observations on the U.S. Atlantic continental slope - variation in time and space: Marine Geology, v. 29, p. 209-219.

MCGREGOR, B.A., BENNETT, R.H., and LAMBERT, D.N., 1979, Bottom processes, morphology and geotechnical properties of the continental slope south of Baltimore Canyon: Applied Ocean Research, v. 1, p. 177-187.

MIDDELBURG, J.J., SOETAERT, K., and HERMAN, P.M.J., 1997, Empirical relationships for use in global diagenetic models: Deep-Sea Research I., v. 44, p. 327-344.

MILLER, K.G., MOUNTAIN, G.S., BROWNING, J.V., KOMINZ, M., SUGARMAN, P.J., CHRISTIE-BLICK, N., KATZ, M.E., and WRIGHT, J.D., 1998, Cenozoic global sea level, sequences, and the New Jersey transect: Results from coastal plain and continental slope drilling: Reviews of Geophysics, v. 36, p. 569-601.

MITCHELL, N.C., 1995, Diffusion transport model for pelagic sediments on the Mid-Atlantic Ridge: Journal of Geophysical Research, v. 100, p. 19,991-20,009.

MITCHELL, N.C., 1996, Creep in pelagic sediments and potential for morphologic dating of marine fault scarps: Geophysical Research Letters, v. 23, p. 483-486.

MITCHELL, N.C., and HUTHNANCE, J.M., 2007, Comparing the smooth, parabolic shapes of interfluves in continental slopes to predictions of diffusion transport models: Marine Geology, v. 236, p. 189-208.

NERC, 2001, Ocean Margin Exchange (OMEX) Project: OMEX-II Project Data set: Liverpool, British Oceanographic Data Centre (Natural Environment Research Council, UK).

OU, H.W., and MAAS, L.R.M., 1988, Tides near a shelf-slope front: Continental Shelf Research, v. 6, p. 729-736.

PANTIN, H.M., and EVANS, C.D.R., 1984, The Quaternary history of the central and southwestern Celtic Sea: Marine Geology, v. 57, p. 259-293.

PENN, B.S., and HARBAUGH, J.W., 1999, The role of positive feedback in the development of interval oscillations for a simple, tightly coupled, nearshore depositional model, in Numerical Experiments in Stratigraphy: Recent Advances in Stratigraphic and Sedimentologic Computer Simulations, eds., J. W. Harbaugh, W.

L. Watney, E. Rankey, R. Slingerland, R. Goldstein, and E. Franseen: SEPM, Special Publication 62, p. 265-270.

PÉREZ GUSSINYÉ, M., 2000, Continental rifting and break-up at the west Iberian margin: an integrated geophysical study: *unpublished thesis, PhD, Christian-Albrechts University*, Kiel, Germany, 183 p.

PIRMEZ, C., PRATSON, L.F., and STECKLER, M.S., 1998, Clinoform development by advection-diffusion of suspended sediment: Modeling and comparison to natural systems: Journal of Geophysical Research, v. 103, p. 24,141-24,157.

POPPE, L.J., HALL, R.E., COUSMINER, H.L., STANTON, R.W., and STEINKRAUS, W.E., 1990, Biostratigraphy, lithofacies and paleoenvironments of the Gulf 718-1 Well, U.S. Mid-Atlantic outer continental shelf: Marine Geology, v. 92, p. 27-50.

QUIQUEREZ, A., ALLEMAND, P., DROMART, G., and GARCIA, J.-P., 2004, Impact of storms on mixed carbonate and silliclastic shelves: insights from combined diffusive and fluid flow transport stratigraphic forward model: Basin Research, v. 16, p. 431-449.

RIVENAES, J.C., 1992, Application of a dual-lithology, depth dependent diffusion equation in stratigraphic simulation: Basin Research, v. 4, p. 133-146.

RIVENAES, J.C., 1997, Impact of sediment transport efficiency on large-scale sequence architecture: results from stratigraphic computer simulation: Basin Research, v. 9, p. 91-105.

SANFORD, L.P., and MAA, J.P.-Y., 2001, A unified erosion formulation for fine sediments: Marine Geology, v. 179, p. 9-23.

SANFORD, M.W., KUEHL, S.A., and NITTROUER, C.A., 1990, Modern sedimentary processes in the Wilmington Canyon area, United States east coast: Marine Geology, v. 92, p. 205-226.

SANGREE, J.B., and WIDMIER, J.M., 1977, Seismic stratigraphy and global changes in sea level, o, Seismic interpretation of depositional facies, *in* Payton, C.E., ed., Seismic Stratigraphy: Applications to Hydrocarbon Exploration: Am. Assoc. Petrol. Geol. Mem. 26: Tulsa, Oklahoma, Am. Assoc. Petrol. Geol., p. 165-184.

SCHLAGER, W., and ADAMS, E.W., 2001, Model for the sigmoidal curvature of submarine slopes: Geology, v. 29, p. 883-886.

SCHLEE, J., BEHRENDT, J.C., GROW, J.A., ROBB, J.M., MAATTICK, R.E., TAYLOR, P.T., and LAWSON, B.A., 1976, Regional geologic framework off northeastern United States: American Association of Petroleum Geologists, Bulletin, v. 60, p. 926-951.

SCHLEE, J.S., DILLON, W.P., and GROW, J.A., 1979, Structure of the continental slope off the Eastern United States, *in* Doyle, L.J., and Pilkey, O.H., eds., Geology of Continental Slopes: Society of Economic Paleontologists and Mineralogists, Special Publication 27, p. 95-117.

SCHMIDT, S., VAN WEERING, T.C.E., REYSS, J.-L., and VAN BEEK, P., 2002, Seasonal deposition and reworking at the sediment-water interface on the northwestern Iberian margin: Progress in Oceanography, v. 52, p. 331-348.

SEKINE, M., and PARKER, G., 1992, Bed-load transport on transverse slope. 1.: Journal of Hydraulic Engineering, v. 118, p. 513-535.

SHAW, P.-T., PIETRAFESA, L.J., FLAGG, C.N., HOUGHTON, R.W., and SU, K.-H., 1994, Low-frequency oscillations on the outer shelf in the southern Mid-Atlantic Bight: Deep-Sea Research II, v. 41, p. 253-271.

SHERWIN, T.J., VLASENKO, V.I., STASHCHUK, N., JEANS, D.R.G., and JONES, B., 2002, Along-slope generation as an explanation for some unusually large internal tides: Deep-Sea Research I., v. 49, p. 1787-1799.

SMALL, E.E., ANDERSON, R.S., and HANCOCK, G.S., 1999, Estimates of the rate of regolith production using Be-10 and Al-26 from an alpine hillslope: Geomorphology, v. 27, p. 131-150.

SMITH, W.H.F., and SANDWELL, D.T., 1997, Global sea floor topography from satellite altimetry and ship soundings: Science, v. 277, p. 1956-1962.

SOETAERT, K., HERMAN, P.M.J., MIDDELBURG, J.J., HEIP, C., DESTIGTER, H.S., VAN WEERING, T.C.E., EPPING, E., and HELDER, W., 1996, Modelling ^{210}Pb-derived mixing activity in ocean margin sediments: diffusive versus nonlocal mixing: Journal of Marine Research, v. 54, p. 1207-1227.

SOULSBY, R., 1997, Dynamics of Marine Sands: A Manual for Practical Applications: Thomas Telford, London, 249 p.

SOUTHARD, J.B., and STANLEY, D.J., 1976, Shelf-break processes and sedimentation, *in* Stanley, D.J., and Swift, D.J.P., eds., Marine Sediment Transport and Environmental Management: New York, John Wiley & Sons, p. 351-377.

STANLEY, D.J., ADDY, S.K., and BEHRENS, E.W., 1983, The mudline: variability of its position relative to shelfbreak, *in* Stanley, D.J., and Moore, G.T., eds., The Shelfbreak: Critical Interface on Continental Margins: Tulsa, Oklahoma, Society of Economic Paleontologists and Mineralogists, p. 279-298.

STANLEY, D.J., and WEAR, C.M., 1978, The "mud-line:" an erosion-deposition boundary in the upper continental slope: Marine Geology, v. 28, p. M19-M29.

STECKLER, M.S., MOUNTAIN, G.S., MILLER, K.G., and CHRISTIE-BLICK, N., 1999, Reconstruction of Tertiary progradation and clinoform development on the New Jersey passive margin by 2-D backstripping: Marine Geology, v. 154, p. 399-420.

SYVITSKI, J.P.M., and DAUGHNEY, S., 1992, DELTA2: Delta progradation and basin filling: Computers & Geosciences, v. 18, p. 839-897.

THOMSEN, L., VAN WEERING, T.C.E., and GUST, G., 2002, Processes in the benthic boundary layer at the Iberian continental margin and their implication for carbon mineralization: Progress in Oceanography, v. 52, p. 315-329.

VAIL, P.R., MITCHUM, R.M., and THOMPSON, S., 1977, Seismic stratigraphy and global changes of sea level; Part 4, Global cycles of relative changes of sea level, *in* Payton, C.E., ed., Seismic stratigraphy - Applications to Hydrocarbon Exploration. American Association Petroleum Geologists, Memoir 26, p. 83-97.

VAN SICKEL, W.A., KOMINZ, M.A., MILLER, K.G., and BROWNING, J.V., 2004, Late Cretaceous and Cenozoic sea-level estimates: backstripping analysis of borehole data, onshore New Jersey: Basin Research, v. 16, p. 451-465.

VAN WEERING, T.C.E., DE STIGTER, H.C., BOER, W., and DE HAAS, H., 2002, Recent sediment transport and accumulation on the NW Iberian margin: Progress in Oceanography, v. 52, p. 349-371.

VITORINO, J., OLIVEIRA, A., JOUANNEAU, J.M., and DRAGO, T., 2002, Winter dynamics on the northern Portuguese shelf. Part 1: physical processes: Progress in Oceanography, v. 52, p. 129-153.

WESSEL, P., and SMITH, W.H.F., 1991, Free software helps map and display data: Eos, Transactions, American Geophysical Union, v. 72, p. 441.

WOLFE, C.J., MCNUTT, M.K., and DETRICK, R.S., 1994, The Marquesas archipelagic apron: Seismic stratigraphy and implications for volcano growth, mass wasting, and underplating: Journal of Geophysical Research, v. 99, p. 13,591-13,608.

XING, J., and DAVIES, A.M., 2002, Influence of wind direction, wind waves, and density stratification upon sediment transport in shelf edge regions: The Iberian shelf: Journal of Geophysical Research, v. 107, p. DOI: 10.1029/2001JC000961.

YAMASAKA, M., IKEDA, S., and KIZAKI, S., 1987, Lateral sediment transport of heterogeneous bed materials: Japanese Society of Civil Engineering, Transactions v. 387, p. 105-114 (in Japanese).

YOKOYAMA, Y., LAMBECK, K., DE DECKKER, P., JOHNSTON, P., and FIFIELD, L.K., 2000, Timing of the Last Glacial Maximum from observed sea-level minima: Nature, v. 406, p. 713-716.

ZHANG, P., MOLNAR, P., and DOWNS, W.R., 2001, Increased sedimentation rates and grain sizes 2-4 Myr ago due to the influence of climate change on erosion rates: Nature, v. 410, p. 891-897.

Electronic Supplements

ES1. GRAVITY EFFECT ON SANDY BEDLOAD

The following section outlines present understanding of how gravity affects bedload transport flux. The initial models based on Bagnold's (1963) work are described first, because they provide a useful framework for understanding the influence on bed morphology. Bagnold's approach is considered valid only for highly developed, dense bedloads (Leeder 1979), so more recent work describing effects of individual saltating particles is also described.

For a simple horizontal sandy bed affected by a strong uniform, steady current, Bagnold's original formula is still considered reasonably accurate (Soulsby 1997):

$$Q_b \text{ (kg/m/s)} \propto \tau_b^{1/2}(\tau_b - \tau_0); \qquad \tau_b > \tau_0 \quad \text{(ES1)}$$

where τ_b is the shear stress imposed by bottom current on the bed and τ_0 is a threshold stress for sediment motion (the symbol "$\propto$" means "is proportional to", i.e., constants are left out for simplicity). Equation ES1 follows a similar relation found empirically in earlier flume experiments (Meyer-Peter and Muller 1948). Because the bed shear stress $\tau_b = C_d \rho_w U^2$, where C_d is a bed friction factor, ρ_w is seawater density, and U is mean flow velocity above the bottom boundary layer, Equation ES1 can also be written $Q_b \propto C_d^{3/2} U(U^2 - U_0^2)$ where U_0 corresponds with τ_0. Thus, for a bed of uniform and unchanging C_d, flow significantly faster than U_0 leads to approximately $Q_b \propto U^3$.

Nielsen (1992) described how Equation ES1 could arise based on Bagnold's original arguments. The mobile bedload imposes a normal stress σ_e on the lower immobile bed equal to the submerged weight of the bedload (allowing for buoyancy):

$$\sigma_e = (\rho_g - \rho_w) g \int_0^\infty C(z)\,dz \qquad \text{(ES2)}.$$

where ρ_g is the sediment grain density, g is the gravitational acceleration, and C is the sediment volumetric density. Assuming that a simple Mohr-Coulomb yield criterion applies to the top of the immobile layer (dashed line in Figure 1A) and that the shear stress at that level equals the shear stress imposed by the current (i.e., the solid phase acquires the current shear stress perfectly through grain to grain collisions (Bagnold 1963)), the flow-imposed shear stress is

$$\tau = \tau_0 + \sigma_e \tan\phi_s \qquad \text{(ES3)}.$$

where ϕ_s is the sediment's angle of internal friction. The amount of bedload mobilized then relates to the excess imposed shear stress:

$$\int_0^\infty C(z)dz = \frac{\tau_b - \tau_0}{(\rho_g - \rho_w)g\tan\phi_s} \qquad \text{(ES4)}.$$

Thus, the term (τ_b-τ_0) in Equation ES1 could arise from friction - a larger imposed stress mobilizes a greater amount of sand, leading to greater bedload flux. Nielsen noted that too few data are available on the velocities of individual grains to then predict the resulting bedload flux, but the fact that various flux measurements follow Equation ES1 (Bagnold 1980; Nielsen 1992) suggests that mean particle velocities scale with flow shear velocity, as found by tracking particles using high-speed film (Fernandez Luque and van Beek 1976).

The effect of sloping beds is illustrated in Figure 1 (shear stress due to the current is omitted for simplicity). For a longitudinal gradient, the normal stress in Equation ES2 is modified by the factor $\cos\gamma$ and the total shear stress acting on the threshold surface includes the component of bedload weight. Equation ES3 then becomes (Bagnold 1963):

$$\tau = \tau_0 + (\tan\phi_s + \tan\gamma)\cos\gamma(\rho_g - \rho_w)g\int_0^\infty C(z)dz \qquad \text{(ES5)}.$$

(γ here is negative for a down-gradient.) The amount of bedload of Equation ES4 should then be modified, with greater amounts mobilized on down-gradients:

$$\int_0^\infty C(z)dz = \frac{\tau_b - \tau_0}{(\tan\phi_s + \tan\gamma)\cos\gamma(\rho_g - \rho_w)g} \quad \text{(ES6)}.$$

Bagnold (1963) derived Equation ES1 by assuming that the power expended by the shearing bedload was a simple proportion of the power expended by the current. Bagnold's energetics argument was extended to arbitrary slopes (Bailard and Inman 1981; Huthnance 1982a, 1982b) by assuming that the flux magnitude is proportional to the current's power expenditure but flux direction is governed by the vectorally combined stresses due to the current and down-gradient component of bedload weight. The bedload flux $\mathbf{Q_b}$ is then:

$$\mathbf{Q_b} = S\,|\mathbf{u}|^2(\mathbf{u}\text{-}\lambda|\mathbf{u}|\nabla\mathbf{H})/g \qquad \text{(ES7)}$$

where S is a constant, $\lambda = 1/\tan\phi_s$ and $\nabla\mathbf{H}$ is bed gradient (bold symbols represent vectors and |...| the vector magnitude).

Criticisms have been made concerning Bagnold's approach. In his model, fluid momentum is transferred to moving particles so that the fluid shear stress becomes insignificant at the base of the mobile layer. This only occurs, however, if the bedload is well-developed, otherwise the bedload is better described as isolated saltating particles than as a continuous layer (McEwan et al. 1999; Niño and Garcia 1998; Seminara et al. 2002). Saltation models of varying complexity have been developed (McEwan et al. 1999; Niño and Garcia 1994; Niño and Garcia 1998; Wiberg and Smith 1985, 1989), which variously incorporate particle extraction from the bed, trajectory, rebound or deposition, and dislodgement of bed particles. Trajectories are potentially affected by lift caused by fluid shear or particle rotation (Leeder 1979). Despite their

complexity, these models can reproduce the variations in Equation ES1 remarkably well (e.g., McEwan et al. 1999).

Sekine and Parker (1992) summarized models of bedload on transverse slopes. They suggested that the components of flux down-gradient q_n and in the direction of the current q_s can be separated. If there is no current down-gradient, their ratio is

$$q_n/q_s = -B \tan\gamma; \quad B = B_0(\tau_c/\tau_b)^m \qquad \text{(ES8)}.$$

Depending on the model, the coefficient B_0 incorporates the sand friction coefficient and other parameters. The different models summarized by Sekine and Parker (Engelund 1974; Hasegawa 1981; Ikeda 1982; Kikkawa et al. 1976; Parker 1984; Struiksma et al. 1985), their own results of numerical simulations of saltation, and a more recent model based on entrainment rates varying with shear stress (Parker et al. 2003) predict m = 0 to 1.0. If $q_s \propto \tau_b^{1.5}$ (Equation ES1, omitting the threshold for simplicity), such values of m imply that the down-gradient flux variation lies between $q_n \propto \tau_b^{1.5}$ (i.e., $q_n \propto u^3$) and $q_n \propto \tau_b^{0.5}$ ($q_n \propto u^1$). The wind-tunnel data of Ikeda (1982) and recent model of Parker et al. (2003) are consistent with $q_n \propto \tau_b^{1.0}$ ($q_n \propto u^2$) for large τ_b.

Given the diversity of theoretical predictions, experiments are needed to inform this question, but few are available and most were carried out with longitudinal gradients. Damgaard and co-workers (Damgaard et al. 2003; Damgaard et al. 1997) used a recirculating flume in which flow rate was held fixed but the longitudinal gradient varied. In the first set, fine sand (median diameter d_{50} = 208 μm or ϕ = 2.3) was injected into the base of the flume with a piston controlled such that the injection rate exactly matched removal as bedload. Bedload fluxes derived from sand pickup rate are shown in Figure 2A for three different sets of experiments made with different flow

rates. They show the expected increasing flux with increasing down-slope gradient, with an abrupt increase towards the sand angle of repose.

In their second study at higher flow rates (Damgaard et al. 2003), sediment-trap measurements (representing largely bedload) show a systematic variation with bed gradient. Ripples, however, formed on the bed, significantly affecting suspended sediment fluxes because of sand thrown into suspension at ripple crests. Hence, suspended sediment fluxes (gray-filled circles in Figure 2B) are varied and peak at -5° rather than at maximum gradient. The effect of ripples was complex because different ripple morphologies formed at different bed gradient, leading to varied suspension. Their flow speed of 0.35 m/s measured 13 cm above bed is comparable with maximum speeds measured near the shelf edge (Huthnance et al. 2002). Considering that ripples are observed around the shelf edge (Yorath et al. 1979), varied suspension could be a further complication, but Figure 2B nevertheless shows a general tendency for fluxes to increase with increasing down-gradient.

Further experiments (Fernandez Luque and van Beek 1976; Smart 1984) documented effects of longitudinal gradients. In Smart's experiment, flux increased with $S^{0.6}$ (where S is bed gradient) but included some suspended transport. Fernandez Luque and van Beek's experiments recorded an effect of gradient on the threshold of motion, and bedload flux correlated moderately well with excess stress corrected for the gradient effect.

Japanese experimental results with transverse gradients (Hasegawa 1981; Yamasaka et al. 1987) shown in Sekine and Parker (1992) are reproduced in Figure 2C (those of Hasegawa were carried out in water whereas those of Yamasaka et al. were carried out in air). Based on Equation ES10, the trend in the data should reveal the

value of the exponent m. The main group of data were claimed (Sekine and Parker 1992) to be consistent with $m = 0.25$, which implies $q_n \propto t_b^{1.25}$ ($q_n \propto u^{2.5}$).

The theoretical and experimental results therefore suggest that bedload flux should be affected by bed gradient, with a component down-gradient, $Q_b = -K|\nabla \mathbf{H}|$. Although not well constrained, the Japanese data suggest that the dependence of K on current speed u probably lies between $K \propto u^2$ and $K \propto u^3$. If threshold effects are also considered, a variation $K \propto (u\text{-}u_o)^2$ could produce morphological results similar to $K \propto u^3$. As the published current meter data do not allow threshold effects to be fully accounted for, we have compared current variations with morphology assuming that K lies between $K \propto u^2$ and $K \propto u^3$, but threshold effects may need to be considered in more accurate interpretations.

BAGNOLD, R.A., 1963, Mechanics of marine sedimentation, *in* Hill, M.N., ed., The Sea, 3: New York, Wiley, p. 507-528.

BAGNOLD, R.A., 1980, An empirical correlation of bedload transport rates in flumes and natural rivers: Royal Society, Proceedings, v. 372A, p. 453-473.

BAILARD, J.A., and INMAN, D.L., 1981, An energetics bedload model for a plane sloping beach: local transport: Journal of Geophysical Research, v. 86, p. 2035-2043.

DAMGAARD, J., SOULSBY, R., PEET, A., and WRIGHT, S., 2003, Sand transport on steeply sloping plane and ripple beds: Journal of Hydraulic Engineering, v. 129, p. 706-719 , DOI: 10.1061/(ASCE)0733-9429(2003)129.:9(706).

DAMGAARD, J.S., WHITEHOUSE, R.J.S., and SOULSBY, R.L., 1997, Bed-load sediment transport on steep longitudinal slopes: Journal of Hydraulic Engineering, v. 123, p. 1130-1138.

ENGELUND, F., 1974, Flow and bed topography in channel bends: American Society of Civil Engineers, Journal of the Hydraulics Division, v. 100, p. 1631-1648.

FERNANDEZ LUQUE, R., and VAN BEEK, R., 1976, Erosion and transport of bed load sediment: Journal of Hydraulics Research, v. 14, p. 127-144.

HASEGAWA, K., 1981, Bank-erosion discharge based on a non-equilibrium theory: Japanese Society of Civil Engineering, Transactions, v. 316, p. 37-52 (in Japanese).

HUTHNANCE, J.M., 1982a, On one mechanism forming linear sand banks: Estuarine, Coastal and Shelf Science, v. 14, p. 79-99.

HUTHNANCE, J.M., 1982b, On the formation of sand banks of finite extent: Estuarine, Coastal and Shelf Science, v. 15, p. 277-299.

HUTHNANCE, J.M., HUMPHERY, J.D., KNIGHT, P.J., CHATWIN, P.G., THOMSEN, L., and WHITE, M., 2002, Near-bed turbulence measurements, stress

estimates and sediment mobility at the continental shelf edge: Progress in Oceanography, v. 52, p. 171-194.
IKEDA, S., 1982, Lateral bed load transport on side slopes: American Society of Civil Engineers, Journal of the Hydraulics Division, v. 108, p. 1369-1373.
KIKKAWA, H., IKEDA, S., and KITAGAWA, A., 1976, Flow and bed topography in curved open channels: American Society of Civil Engineers, Journal of the Hydraulics Division, v. 102, p. 1327-1342.
LEEDER, M.R., 1979, Bedload dynamics: Grain impacts, momentum transfer and derivation of a grain Froude number: Earth Surface Processes, v. 4, p. 291-295.
MCEWAN, I.K., JEFCOATE, B.J., and WILLETTS, B.B., 1999, The grain-fluid interaction as a self-stabilizing mechanism in fluvial bed load transport: Sedimentology, v. 46, p. 407-416.
MEYER-PETER, E., and MULLER, R., 1948, Formulas for bedload transport, paper presented at 2nd IAHR Congress, International Association for Hydraulics Research, Stockholm.
NIELSEN, P., 1992, Coastal bottom boundary layers and sediment transport: Advanced Series on Ocean Engineering, vol. 4: Singapore, World Scientific Publishing.
NIÑO, Y., and GARCIA, M., 1994, Gravel saltation: 2. Modeling: Water Resources Research, v. 30, p. 1915-1924.
NIÑO, Y., and GARCIA, M., 1998, Using Lagrangian particle saltation observations for bedload sediment transport modelling: Hydrological Processes, v. 12, p. 1197-1218.
PARKER, G., 1984, Lateral bed-load transport on side slopes - discussion: Journal of Hydraulic Engineering, v. 110, p. 197-199.
PARKER, G., SEMINARA, G., and SOLARI, L., 2003, Bed load at low Shields stress on arbitrarily sloping beds: Alternative entrainment formulation: Water Resources Research, v. 39, p. doi:10.1029/2001WR001253.
SEKINE, M., and PARKER, G., 1992, Bed-load transport on transverse slope. 1.: Journal of Hydraulic Engineering, v. 118, p. 513-535.
SEMINARA, G., SOLARI, L., and PARKER, G., 2002, Bed load at low Shields stress on arbitrarily sloping beds: Failure of the Bagnold hypothesis: Water Resources Research, v. 38, p. Art no. 1249, doi:10.1029/2001WR000681.
SMART, G.M., 1984, Sediment transport formula for steep channels: Journal of Hydraulics Engineering, v. 110, p. 267-276.
SOULSBY, R., 1997, Dynamics of marine sands, a manual for practical applications, Thomas Telford, 249 p.
STRUIKSMA, N., OLESEN, K.W., FLOKSTRA, C., and DE VRIEND, H.J., 1985, Bed deformation in curved alluvial channels: Journal of Hydraulics Research, v. 23, p. 57-79.
WIBERG, P.L., and SMITH, J.D., 1985, A theoretical model for saltating grains in water: Journal of Geophysical Research, v. 90, p. 7341-7354.
WIBERG, P.L., and SMITH, J.D., 1989, Model for calculating bed load transport of sediment: Journal of Hydraulic Engineering, v. 115, p. 101-123.
YAMASAKA, M., IKEDA, S., and KIZAKI, S., 1987, Lateral sediment trasnport of heterogeneous bed materials: Japanese Society of Civil Engineering, Transactions, v. 387, p. 105-114 (in Japanese).

YORATH, C.J., BORNHOLD, B.D., and THOMSON, R.E., 1979, Oscillation ripples on the northeast Pacific continental shelf: Marine Geology, v. 31, p. 45-58.

1
2

ES2: CURRENT-METER STATION LIST AND VALUES

Station ID	Latitude (degrees N)	Longitude (degrees W)	Depth (m)	Measure-ment altitude (m)	Dura-tion (days)	Mean speed (cm/s)	Source	Symbol in Fig. 4
USA Atlantic margin								
SEEP-5/1983[1]	39.805	70.9217	1250	10	197	6.1	Csanady et al. (1988)	square (solid)
SEEP-5/1984[1]	39.805	70.9217	1250	10	173	5.6	Csanady et al. (1988)	square (solid)
NASACS-SA[1]	40.08	68.5583	485	7	148	8.	Butman et al. (1988)	diamond (solid)
NASACS-SE[1]	39.8967	70.0617	491	7	141	9.9	Butman et al. (1988)	diamond (solid)
NASACS-SE[1]	39.8967	70.0617	504	7	244	6.2	Butman et al. (1988)	diamond (solid)
NASACS-SF[1]	39.9617	70.015	202	7	98	13.8	Butman et al. (1988)	diamond (solid)
NASACS-SF[1]	39.9617	70.015	204	7	129	11.6	Butman et al. (1988)	diamond (solid)
NASACS-SA[1]	40.08	68.5583	479	6	149	7.9	Csanady et al. (1988)	square (solid)
NASACS-SF[1]	39.9617	70.015	204	7	143	11.6	Csanady et al. (1988)	square (solid)
NASACS-SG[1]	39.8083	70.0833	1150	7	246	8.4	Butman et al. (1988)	diamond (solid)
NASACS-SH[1]	39.842	70.0283	1220	7	171	5.4	Csanady et al. (1988)	square (solid)
MASAR-A[1]	39.704	73.063	225	5	116	12.4	Csanady et al. (1988)	square (solid)
LCI[1]	40.38	67.5517	250	5	148	9.81	Butman et al. (1988)	diamond (solid)
LCI[1]	40.38	67.5517	250	5	146	8.86	Butman et al. (1988)	diamond (solid)
LCI[1]	40.38	67.5517	247	5	125	9.93	Butman et al. (1988)	diamond (solid)
LCI[1]	40.38	67.5517	249	6	157	11.95	Butman et al. (1988)	diamond (solid)
Atlantic data also plotted but not used in the speed-depth regression:								
A[1]	39.48	72.98	59	1.5-2.0	11.92	10.7	McClennen (1973)	plus
C[1]	39.06	74.0767	30	1.5-2.0	8.88	12.	McClennen (1973)	plus
D[1]	38.8467	73.16	74	1.5-2.0	10.79	11.7	McClennen (1973)	plus
B[1]	39.25	72.5667	143	1.5-2.0	10.13	17.8	McClennen (1973)	plus
T[1]	40.1817	69.9717	100	7	117	10.95	Butman et al. (1988)	plus
SEEP-2/1983[1]	40.2417	70.9167	125	5	146	10.3	Csanady et al. (1988)	plus
Aa[1]	39.3917	72.9917	60	-	36	8	Butman (1979)	plus
Ab[1]	39.3917	72.9917	65	-	23	7	Butman (1979)	plus
B[1]	38.7083	73.6333	60	-	68	9	Butman	plus

							(1979)	
Ca[1]	38.5417	73.5083	80	-	36	13	Butman (1979)	plus
Cb[1]	38.5417	73.5083	87	-	14	6	Butman (1979)	plus
MASAR-F[1]	36.836	74.576	1005	100	210	6.5	Csanady et al. (1988)	square (open)
NASACS-SA[1]	40.08	68.5583	475	100	337	10.4	Csanady et al. (1988)	square (open)
NASACS-SD[1]	40.284	67.730	485	100	328	11.4	Csanady et al. (1988)	square (open)
NASACS-SE[1]	39.8967	70.0617	500	100	350	9.5	Csanady et al. (1988)	square (open)
NASACS-SE[1]	39.8967	70.0617	510	100	142	9.9	Csanady et al. (1988)	square (open)
NASACS-SE[1]	39.8967	70.0617	504	100	245	8.8	Csanady et al. (1988)	square (open)
LCI[1]	40.38	67.5517	250	55	148	9.46	Butman et al. (1988)	diamond (open)
LCI[1]	40.38	67.5517	249	50	157	8.97	Butman et al. (1988)	diamond (open)
Iberian Atlantic margin:								
stablecd110[1]	42.6783	9.50833	202	0.21-0.91	18	13	Huthnance et al. (2002)	square (solid)
stablecd114[1]	42.6667	9.50833	200	0.21-0.91	18.5	10	Huthnance et al. (2002)	square (solid)
rcm03192[3]	40.999	9.475	1293	99	730.6	10.62	Malena (WOCE) (2)	star (solid)
rcm02590[3]	42.218	9.509	1338	100	387	3.95	Malena (WOCE) (2)	star (solid)
b0530652[3]	41.315	8.9867	84.0	2.	75.	8.87	OMEX-II(1)	diamond (solid)
b0530720[3]	41.3183	8.9817	84	3.	139.	9.35	OMEX-II(1)	diamond (solid)
-[2]	42.33	9.38	853	0.05-0.4	-	6.6	Thomsen et al. (2002)	circle (solid)
-[2]	42.33	9.38	194	0.05-0.4	-	18.75	Thomsen et al. (2002)	circle (solid)
-[2]	42.33	9.38	97	0.05-0.4	-	27	Thomsen et al. (2002)	circle (solid)
-[2]	43.05	9.52	155	0.05-0.4	-	31.4	Thomsen et al. (2002)	circle (solid)
OTHER W EUROPE ATLANTIC MARGIN								
Hebrides[1]	56.45	9.05	210	0.21-0.91	27	12	Huthnance et al. (2002)	circle (open)
Hebrides[1]	56.46	9.04667	204	0.21-0.91	15	14	Huthnance et al. (2002)	circle (open)
Goban Spur[1]	49.3917	11.6667	879	0.21-0.91	10	11	Huthnance et al. (2002)	circle (open)
Chapelle Bank[1]	47.47	6.54667	388	0.21-0.91	8	17	Huthnance et al. (2002)	circle (open)

"Station ID" is the identifier used in the data sources.
(1) Ocean Margin Exchange (OMEX) Project, OMEX-II Project data set (CD-ROM, British Oceanographic Data Centre, Liverpool, UK (NERC)). Original data attributed to Instituto Hidrografico, Portugal.

(2) Data calculated from current velocity data supplied as part of the WOCE compilation, attributed to ACM27 and ACM28 ("Morena" experiment). Originally collected by scientists of the University of Lisbon and the Spanish Institute of Oceanography. Related publication: Fiúza, A. F. G., Hamann, M., Ambar, I., Díaz del Río, G., González, N., and Cabanas, J. M., 1998, Water masses and their circulation off western Iberia during May 1993: Deep-Sea Res. I., v. 45, p. 1127-1160.

Superscripts in Station ID column refer to the type of measuring instrument:
[1]Mechanical: rotor(s) with direction vane.
[2]Acoustic doppler current profiler.
[3]Unknown.

Notes on accuracy

As the above results include measurements made with different current meters, the relative performance of the different instruments could be a cause for concern. In particular, the mean current measured with mechanical current meters is known to be affected by superimposed oscillating currents, such as from surface waves, because of the finite response time of the rotors and direction vane. The instruments measure the wave current when it adds to the mean current but under-record when the wave-current reverses, leading to a net bias. In one study (Beardsley 1987), when wave currents had root-mean-squared amplitudes equal to half the mean current velocity, the measured current was in error by 10% and greater for larger oscillating current amplitudes. These measurements will also not be particularly representative of the instantaneous current speed (due to both wave and mean current) in such situations. These issues are not expected to affect the arguments in this paper greatly because we are concerned with variations below 150 m where high-frequency oscillating currents tend not to penetrate.

Potential errors in the calibration formulae that have been used at Woods Hole Oceanographic Institution to relate rotor speed to current speed have been noted by Lentz et al. (1995). Their comparison of a mechanical current meter with an acoustic current meter suggested that the error increased linearly to around 2.5 cm/s at a speed of 30 cm/s. If it had affected the results of Csanady et al. (1988) and Butman et al. (1988) (these papers unfortunately lack calibration details), the values in Fig. 5A will have been exaggerated by around 1 cm/s at 10 cm/s mean speed and less at depth. This will have steepened the graph slightly but not sufficiently to affect the arguments in the paper.

REFERENCES

BEARDSLEY, R.C., 1987, A comparison of the vector-averaging current meter and New Edgerton, Germeshausen, and Grier, Inc., vector-measuring current meter on a surface mooring in Coastal Ocean Dynamics Experiment: Journal of Geophsical Research, v. 92, p. 1845-1859.

BUTMAN, B., NOBLE, M., and FOLGER, D.W., 1979, Long-term observations of bottom current and bottom sediment movement on the mid-Atlantic continental shelf: Journal of Geophsical Research, v. 84, p. 1187-1205.

BUTMAN, B., 1988, Downslope Eulerian mean flow associated with high-frequency current fluctuations observed on the outer continental shelf and upper slope along the north-eastern United States continental margin: Implications for sediment transport: Continental Shelf Research, v. 8, p. 811-840.

CSANADY, G.T., CHURCHILL, J.H., and BUTMAN, B., 1988, Near-bottom currents over the continental slope in the Mid-Atlantic Bight: Continental Shelf Research, v. 8, p. 653-671.

HUTHNANCE, J.M., HUMPHERY, J.D., KNIGHT, P.J., CHATWIN, P.G., THOMSEN, L., and WHITE, M., 2002, Near-bed turbulence measurements, stress estimates and sediment mobility at the continental shelf edge: Progress in Oceanography, v. 52, p. 171-194.

LENTZ, S.J., BUTMAN, B., and WILLIAMS, A.J., 1995, Comparison of BASS and VACM current measurements during STRESS: Journal of Atmospheric and Oceanic Technologies, v. 12, p. 1328-1337.

MCCLENNEN, C.E., 1973, New Jersey continental shelf near bottom current meter records and recent sediment activity: Journal of Sedimentary Petrology, v. 43, p. 371-380.

THOMSEN, L., VAN WEERING, T.C.E., and GUST, G., 2002, Processes in the benthic boundary layer at the Iberian continental margin and their implication for carbon mineralization: Progress in Oceanography, v. 52, p. 315-329.

ES3. BOTTOM CURRENTS FROM SHIP ADCP DATA OFF IBERIA

Data were collected with a hull-mounted acoustic Doppler current profiler (ADCP) during a cruise off the Iberian margin shown in Figure ES3 (Huthnance 1997). The ship traversed the margin repeatedly, crossing the 200 m contour at 20 random times with respect to the tidal cycle. Although the 10 day period of the cruise is short compared with some oceanographic variations, these data provide a further indication of how the magnitude of seabed oscillations varies with water depth, in relatively mild June conditions (Huthnance 1997).

The ADCP vector currents were corrected for ship motion and converted to current vector magnitudes. Bathymetry along the ship tracks was derived by interpolating (Smith and Wessel 1990) 50 m contours of the General Bathymetric Chart of the Ocean (GEBCO) above 200 m depth (IOC, IHO and BODC, 2003) along with multibeam bathymetry of the slope (NERC 2001). To derive near-bed current speeds, while allowing for bathymetry inaccuracy due to incomplete coverage, we selected all current data within 60 m of the seabed. The solid line in Figure 5B then represents the median average near-bed current as a function of the local water depth and dotted lines show the inter-quartile range of current speeds.

Because the ADCP averages current data over typically 5 minutes, the trend in Figure 5B excludes effects of long-period surface waves (swell), affecting the shallower depths. Northerly winds during the cruise favored upwelling, and interestingly this should have produced currents decreasing inversely with water depths, similar to those observed. The Ekman surface current is expected to have a volumetric transport flux relative to its underlying water that relates to the wind stress rather than depth, but its squeezing into shallow water leads to stronger currents. If the upwelling flux is Q, the

bottom-layer onshore current is u_b, total depth H, and upper water layer thickness h_u, then the absolute upper-layer flux offshore is $Q - u_b h_u$. The lower-layer flux onshore is $u_b(H - h_u)$. These two transport fluxes cancel at the coast, so combining the above suggests $u_b = Q/H$,, i.e. flow in the lower layer inversely proportional to water depth, similar to that observed in Figure 5B. This analysis applies over shelf depths 100 to 200 m, but friction affects flow in shallower depths and upwelling can occur mid-depth in deeper water.

HUTHNANCE, J.M., 1997, Cruise report RRS Charles Darwin 105, 29 May to 22 June 1997. Ocean Margin Exchange (OMEX II-II): Liverpool, UK, Proudman Oceanographic Laboratory, Cruise Report, No. 26, p. 48.

IOC, IHO and BODC, 2003, Centenary edition of the GEBCO digital atlas, published on CD-ROM on behalf of the Intergovernmental Oceanographic Commission and the International Hydrographic Organization as part of the General Bathymetric Chart of the Oceans, British Oceanographic Data Centre, Liverpool, U.K.

NERC, 2001, Ocean Margin Exchange (OMEX) Project: OMEX-II Project Data set (CD-ROM): Liverpool, British Oceanographic Data Centre (Natural Environment Research Council, UK).

SMITH, W.H.F., and WESSEL, P., 1990, Gridding with continuous curvature splines in tension: Geophysics, v. 55, p. 293-305.

Figure ES3. Path of RRS Charles Darwin during cruise 105 while operating its hull-mounted ADCP.

1

A)

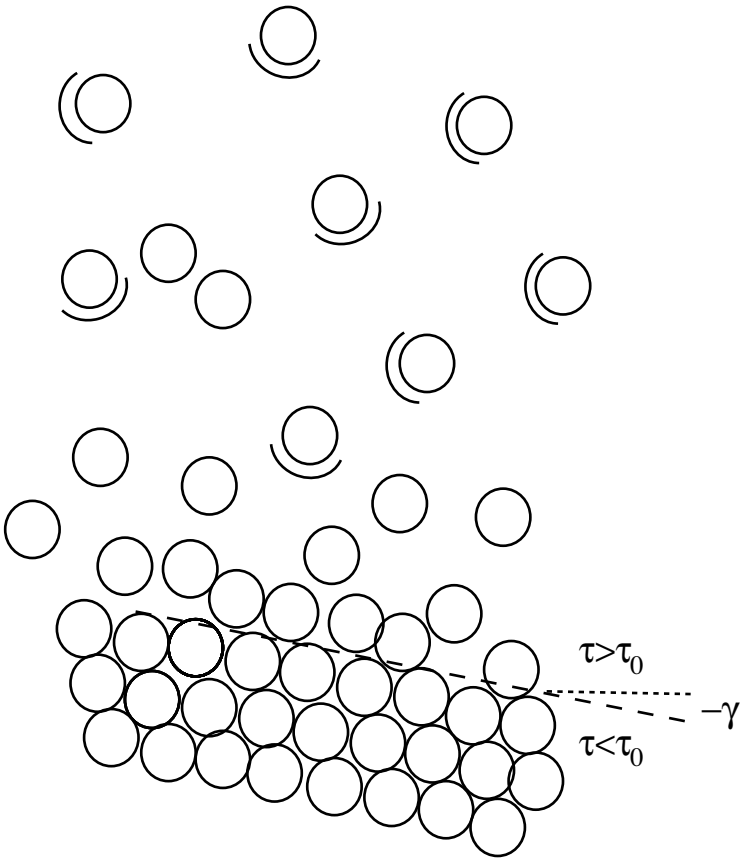

B)

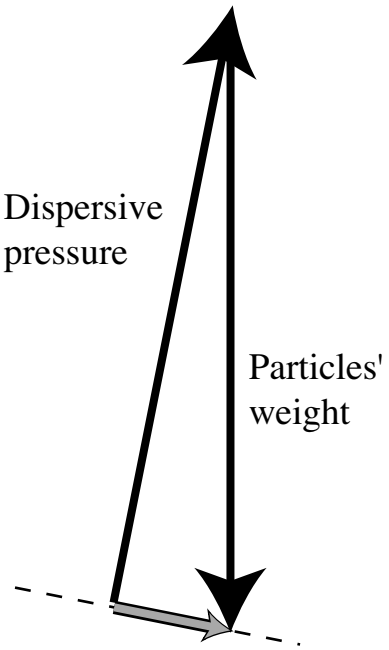

A) Damgaard et al. (1997)

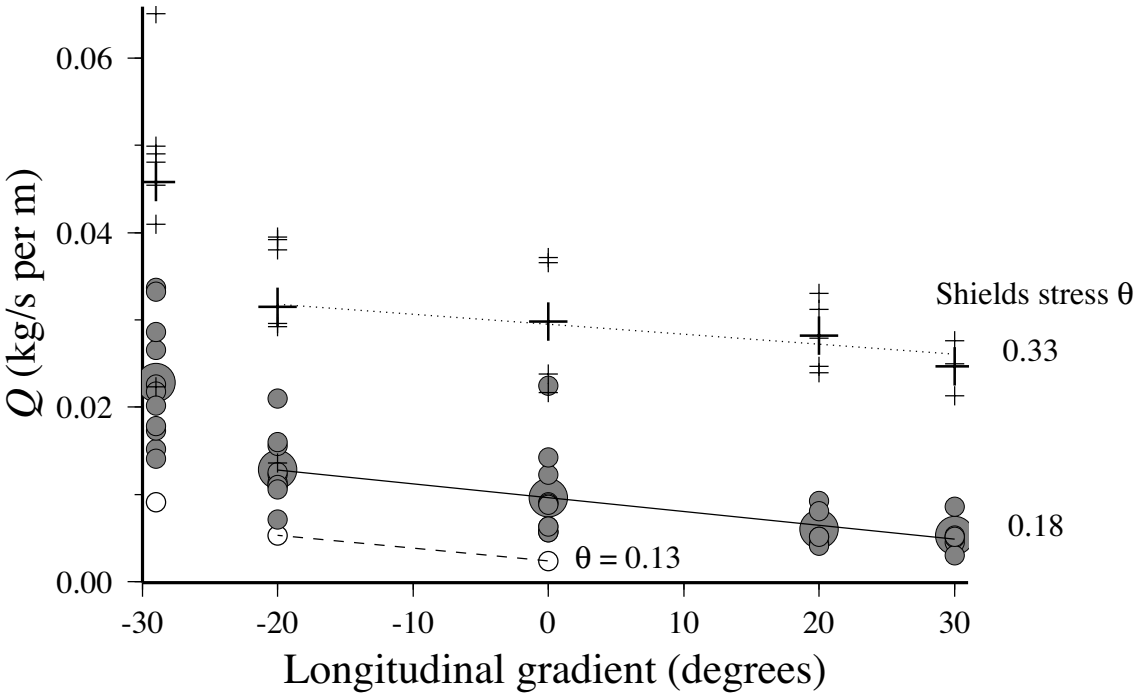

B) Damgaard et al. (2003)

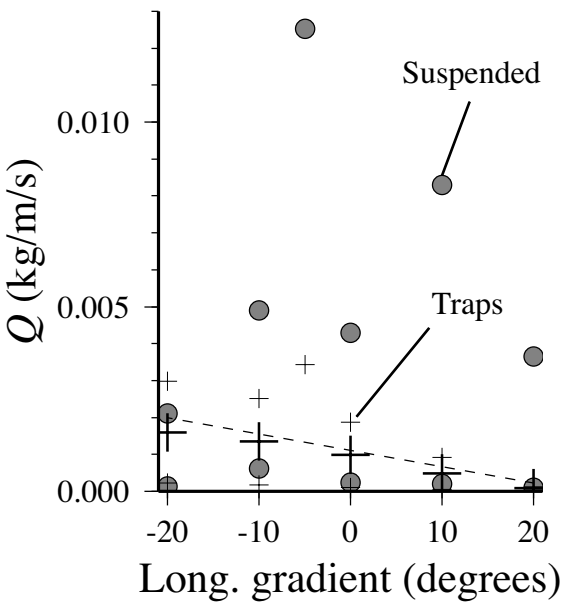

C) Sekine and Parker (1992)

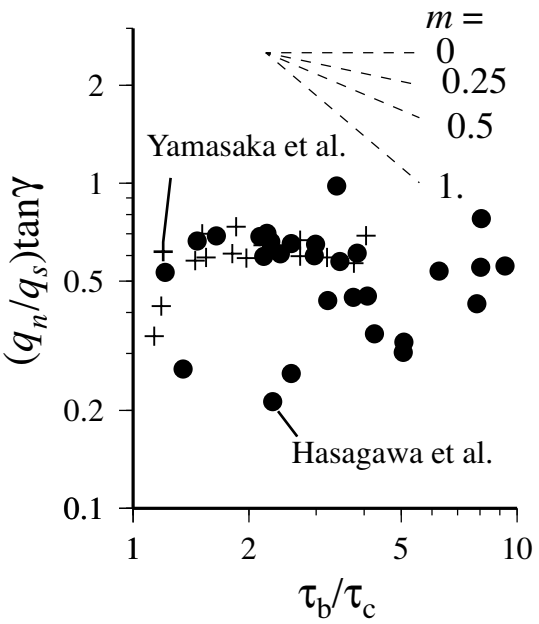

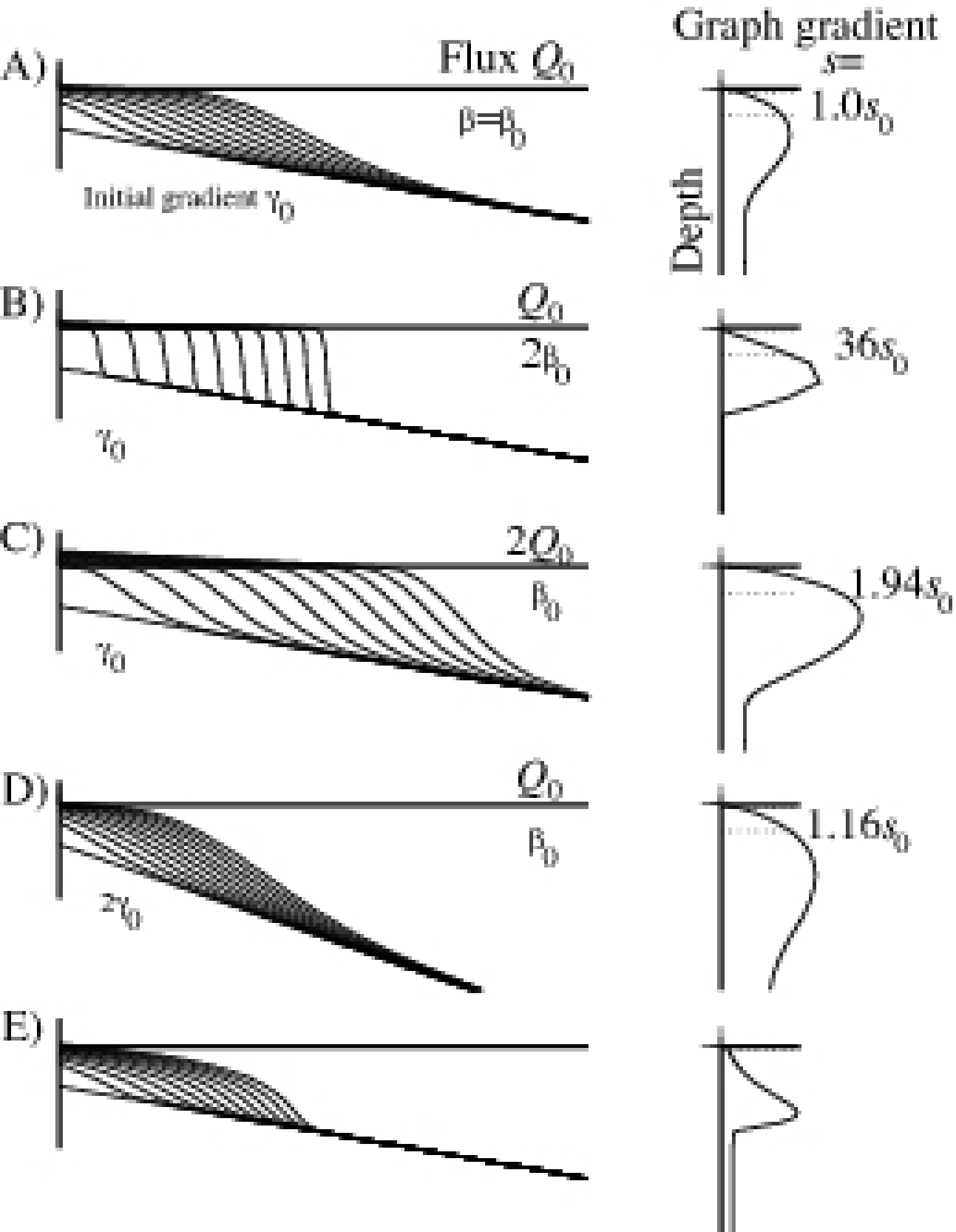
Graph gradient
s=
A)
Flux Q_0
$\beta=\beta_0$
Initial gradient γ_0
Depth
$1.0s_0$
B)
Q_0
$2\beta_0$
γ_0
$36s_0$
C)
$2Q_0$
β_0
γ_0
$1.94s_0$
D)
Q_0
β_0
$2\gamma_0$
$1.16s_0$
E)

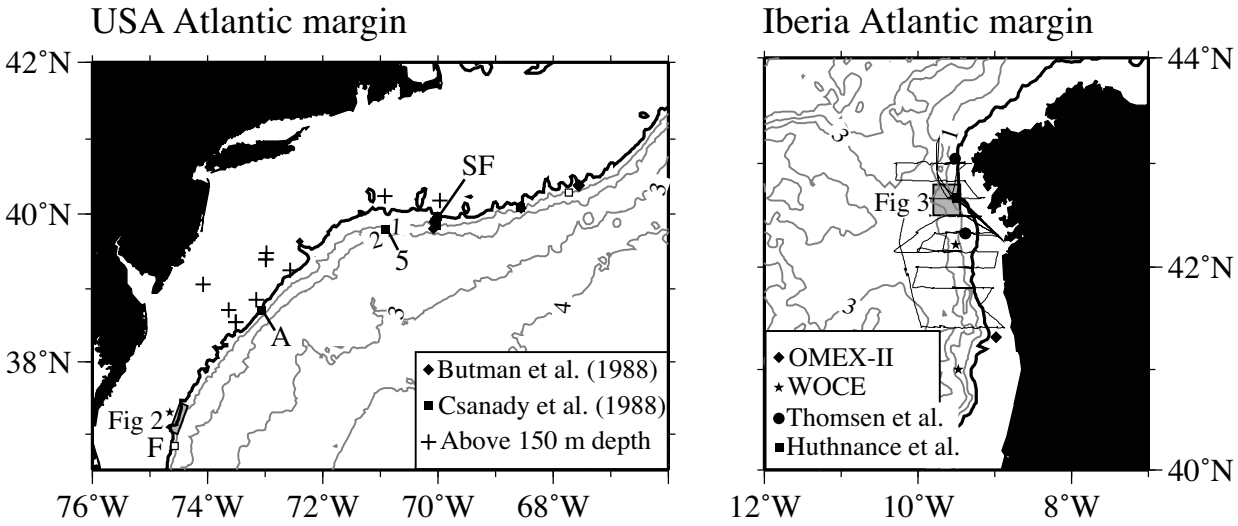
USA Atlantic margin
42°N
40°N
38°N
76°W
74°W
72°W
70°W
68°W
SF
A
F
Fig 2
1
2
5
3
4
Butman et al. (1988)
Csanady et al. (1988)
Above 150 m depth
Iberia Atlantic margin
44°N
42°N
40°N
12°W
10°W
8°W
Fig 3
1
3
OMEX-II
WOCE
Thomsen et al.
Huthnance et al.

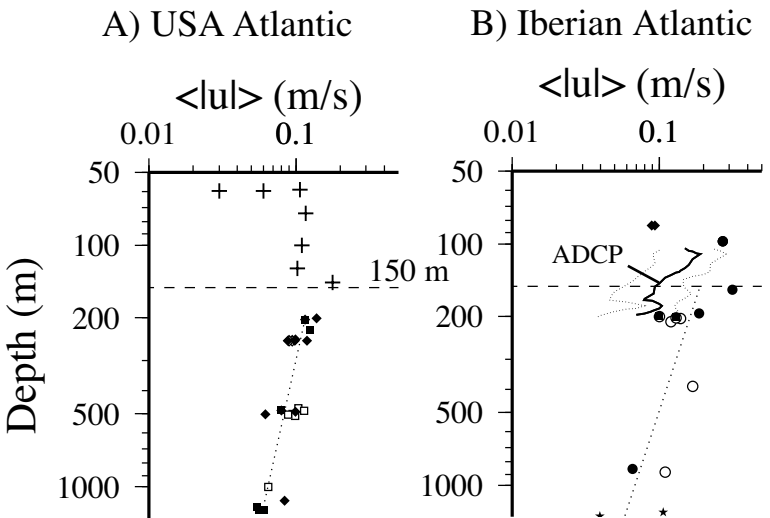
A) USA Atlantic
B) Iberian Atlantic
<|u|> (m/s)
0.01
0.1
50
100
150 m
200
500
1000
Depth (m)
ADCP

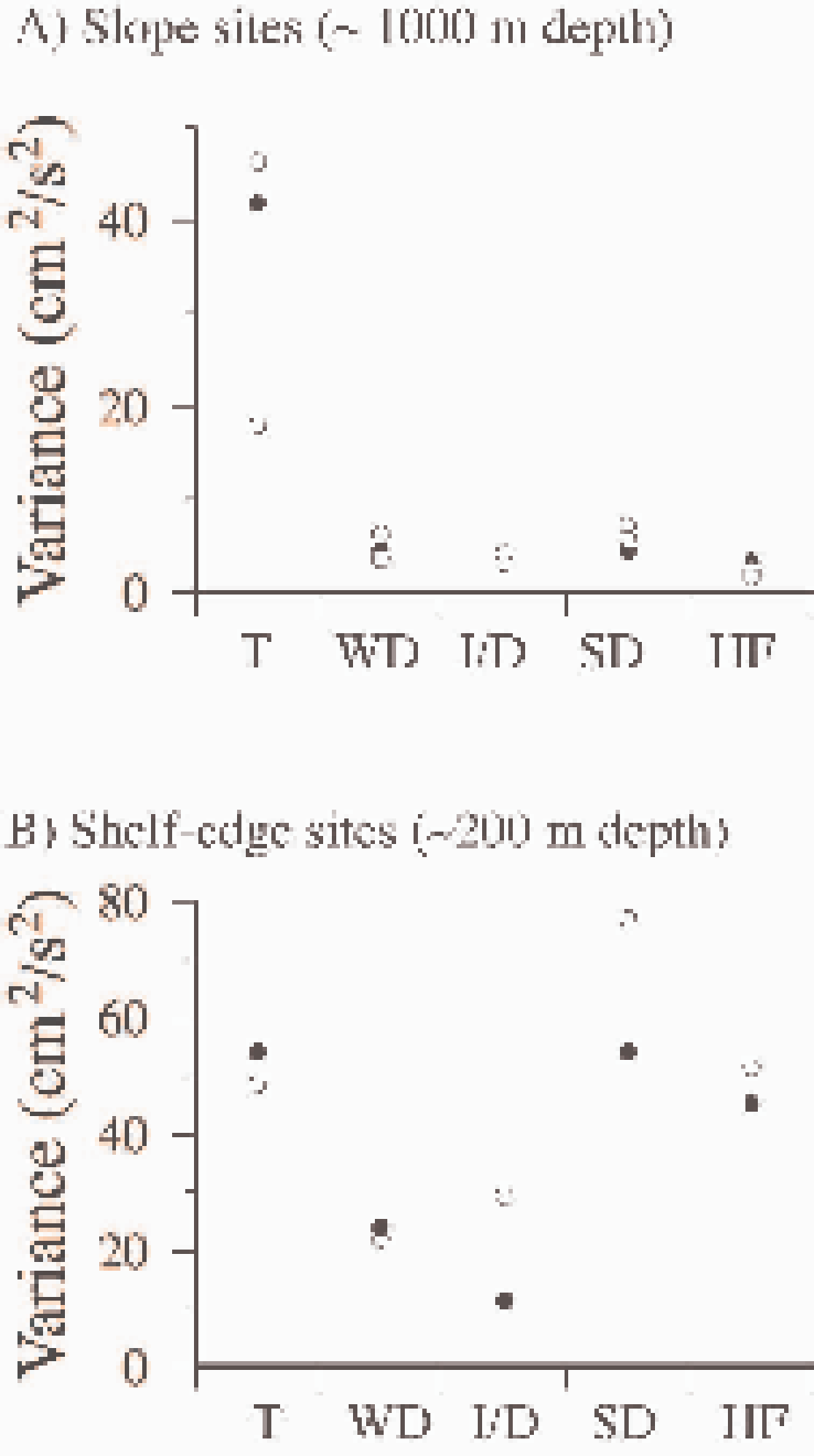
A) Slope sites (~ 1000 m depth)
Variance (cm 2/s2)
0
20
40
T
WD
I/D
SD
HF
B) Shelf-edge sites (~200 m depth)
Variance (cm 2/s2)
0
20
40
60
80
T
WD
I/D
SD
HF

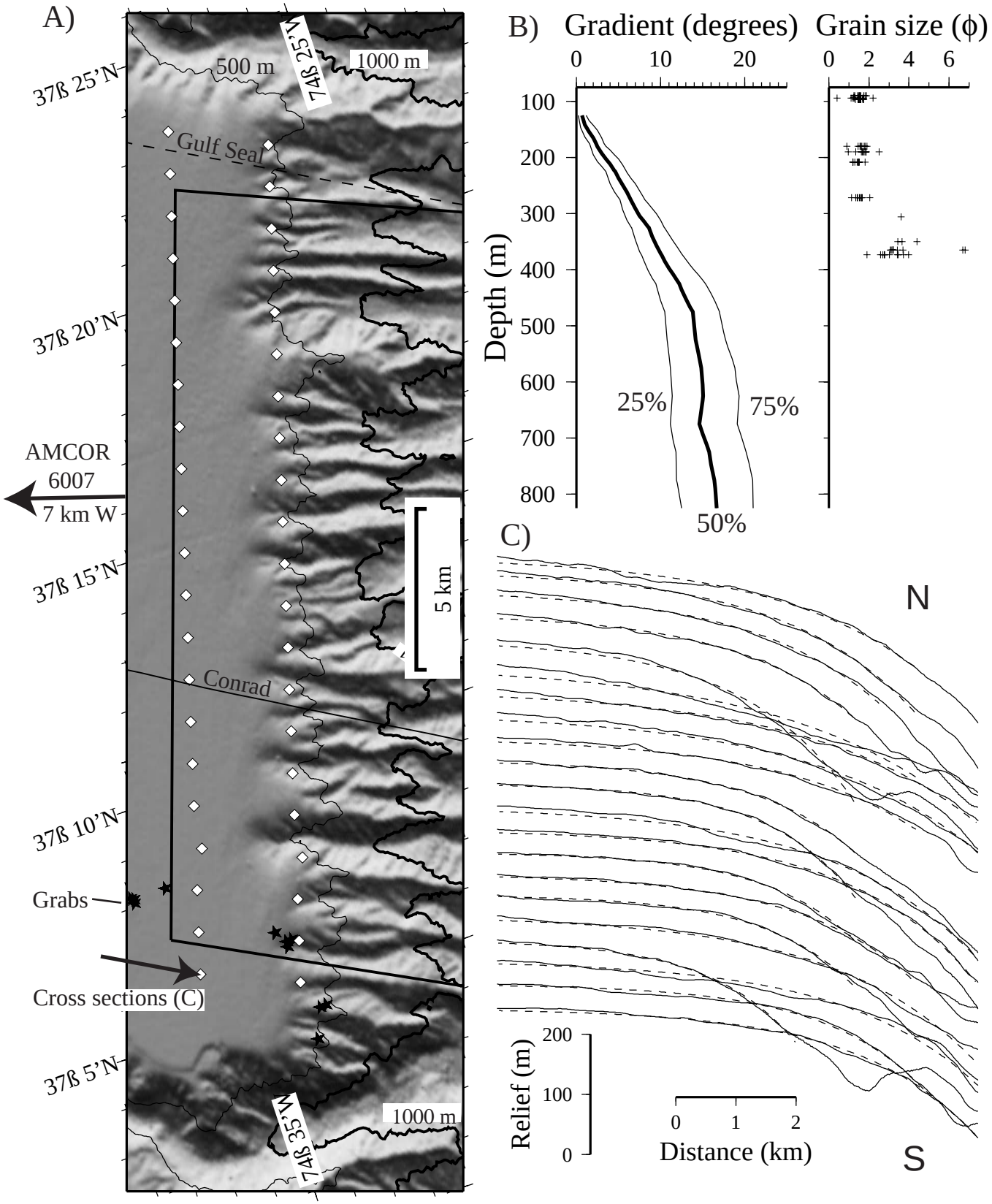
A)
37ß 25'N
37ß 20'N
37ß 15'N
37ß 10'N
37ß 5'N
74ß 25'W
74ß 35'W
500 m
1000 m
1000 m
Gulf Seal
Conrad
AMCOR
6007
7 km W
5 km
Grabs
Cross sections (C)
B)
Gradient (degrees)
Grain size (ϕ)
0
10
20
0
2
4
6
100
200
300
400
500
600
700
800
Depth (m)
25%
75%
50%
C)
N
S
Relief (m)
200
100
0
0
1
2
Distance (km)

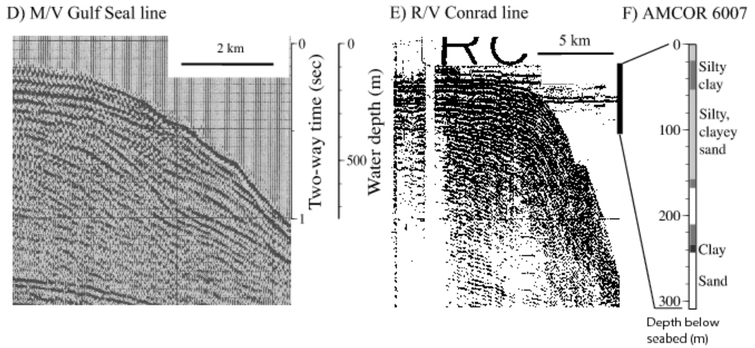
D) M/V Gulf Seal line
2 km
0
500
Two-way time (sec)
0
Water depth (m)
E) R/V Conrad line
5 km
F) AMCOR 6007
0
100
200
300
Silty clay
Silty, clayey sand
Clay
Sand
Depth below seabed (m)

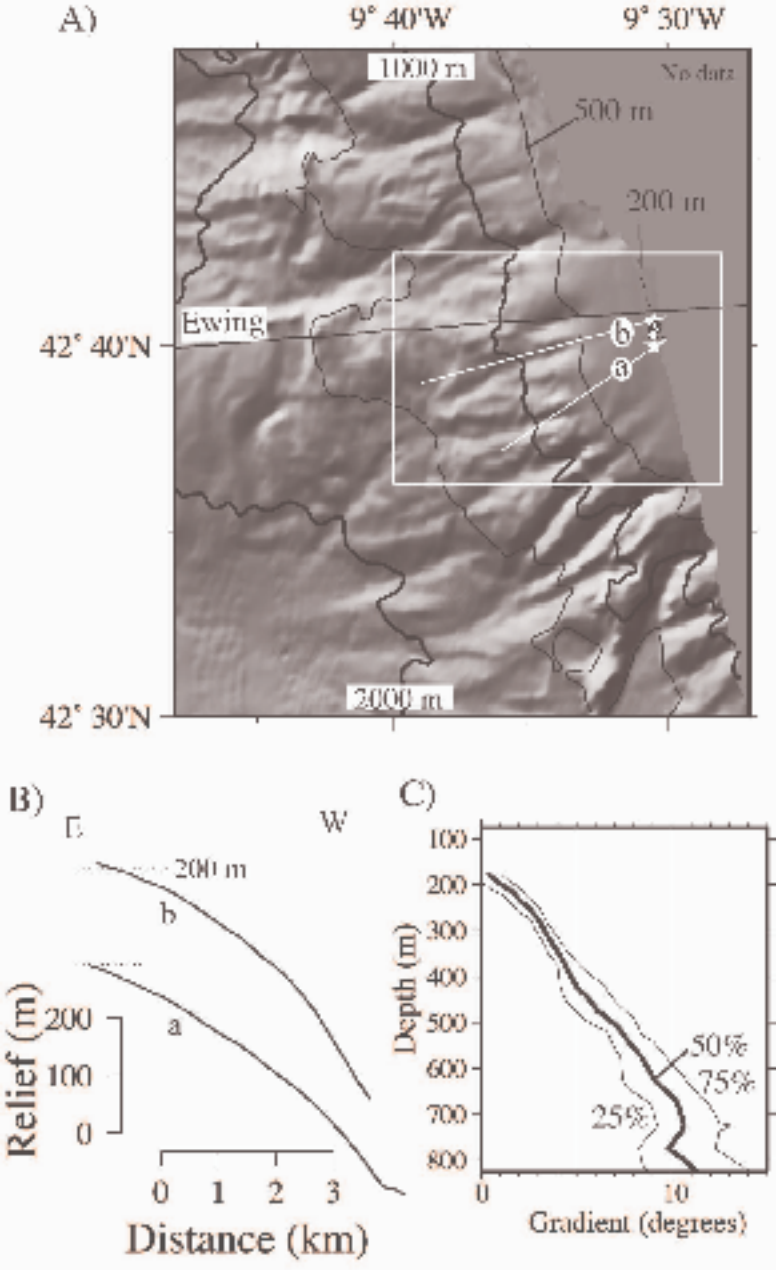
A)
9° 40'W
9° 30'W
1000 m
No data
500 m
200 m
Ewing
42° 40'N
b
a
2
42° 30'N
2000 m
B)
E
W
200 m
b
a
Relief (m)
200
100
0
0
1
2
3
Distance (km)
C)
Depth (m)
100
200
300
400
500
600
700
800
50%
75%
25%
0
10
Gradient (degrees)

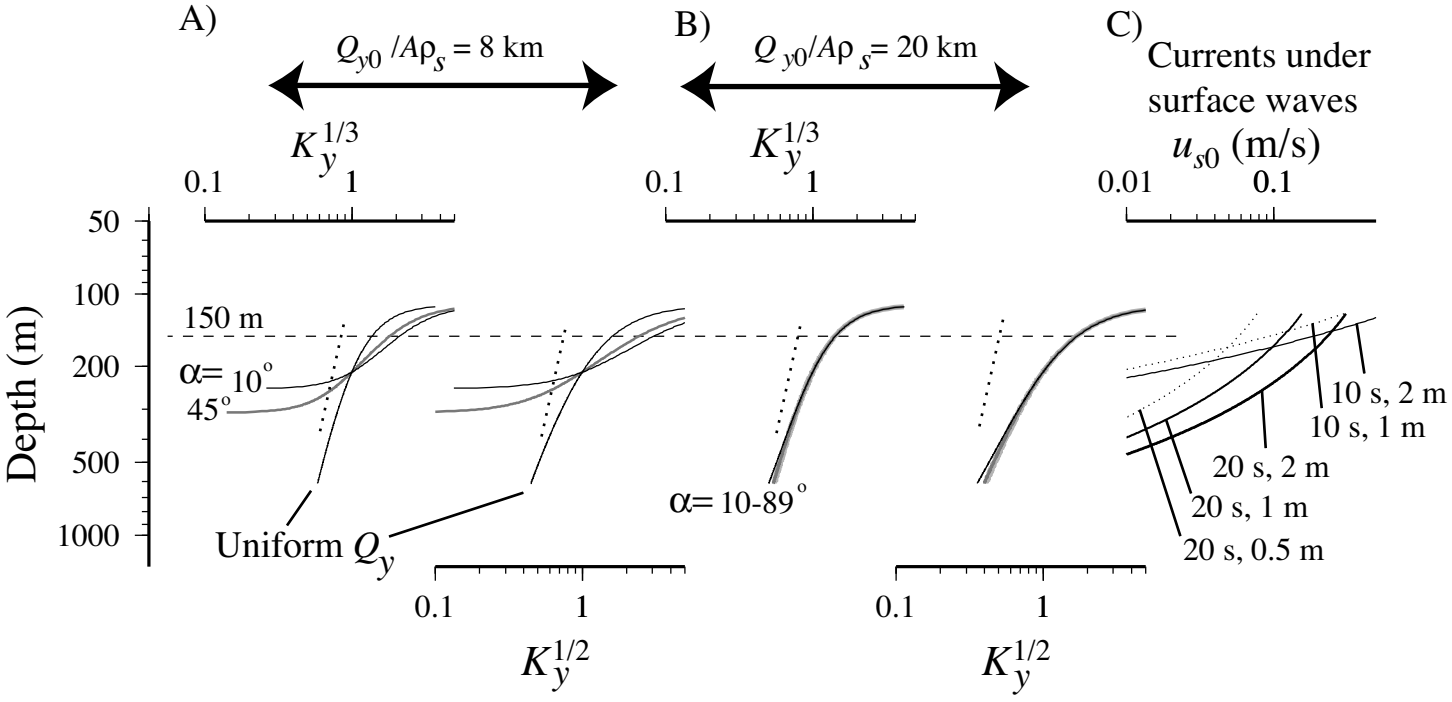
A)
$Q_{y0}/A\rho_s$ = 8 km
$K_y^{1/3}$
0.1
1
B)
$Q_{y0}/A\rho_s$= 20 km
$K_y^{1/3}$
0.1
1
C)
Currents under surface waves
u_{s0} (m/s)
0.01
0.1
Depth (m)
50
100
150 m
200
500
1000
α= 10°
45°
Uniform Q_y
α= 10-89°
10 s, 2 m
10 s, 1 m
20 s, 2 m
20 s, 1 m
20 s, 0.5 m
0.1
1
$K_y^{1/2}$
0.1
1
$K_y^{1/2}$

A) Uniform aggradation

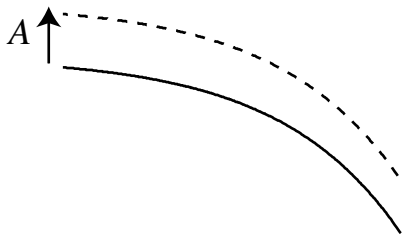

B) Uniform progradation

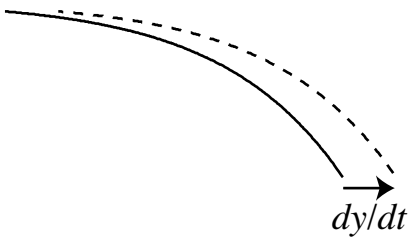

C) Aggradation and progradation

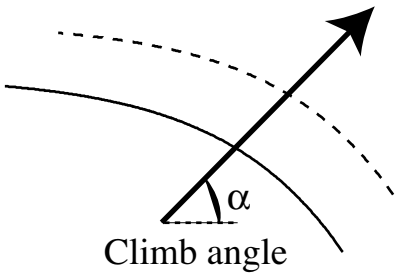

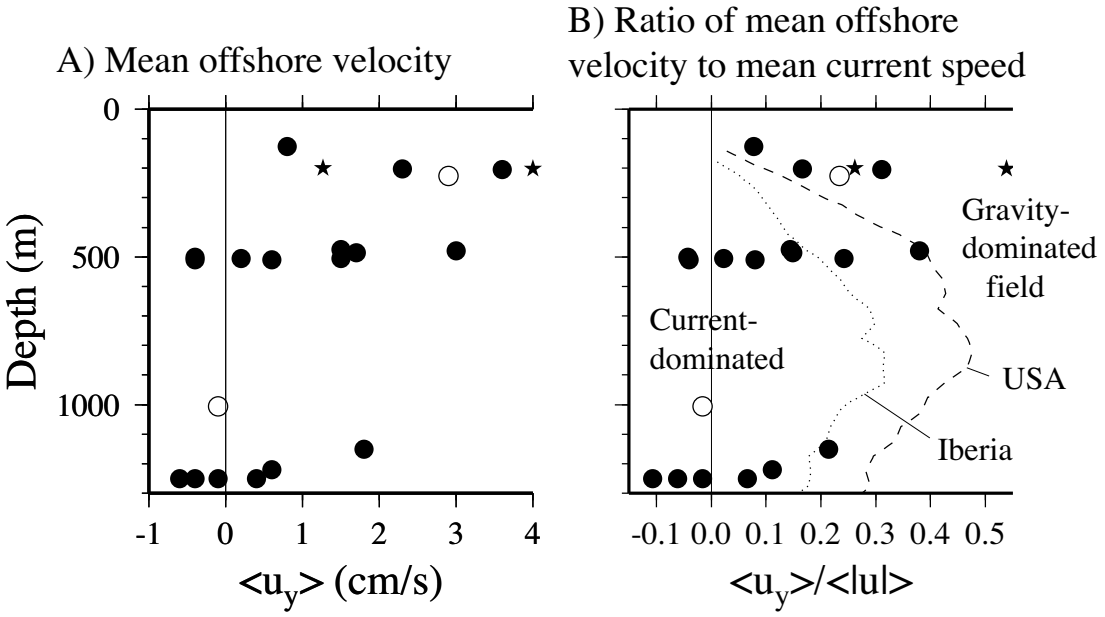
A) Mean offshore velocity
B) Ratio of mean offshore velocity to mean current speed
Depth (m)
0
500
1000
-1
0
1
2
3
4
<u_y> (cm/s)
-0.1
0.0
0.1
0.2
0.3
0.4
0.5
<u_y>/<|u|>
Gravity-dominated field
Current-dominated
USA
Iberia

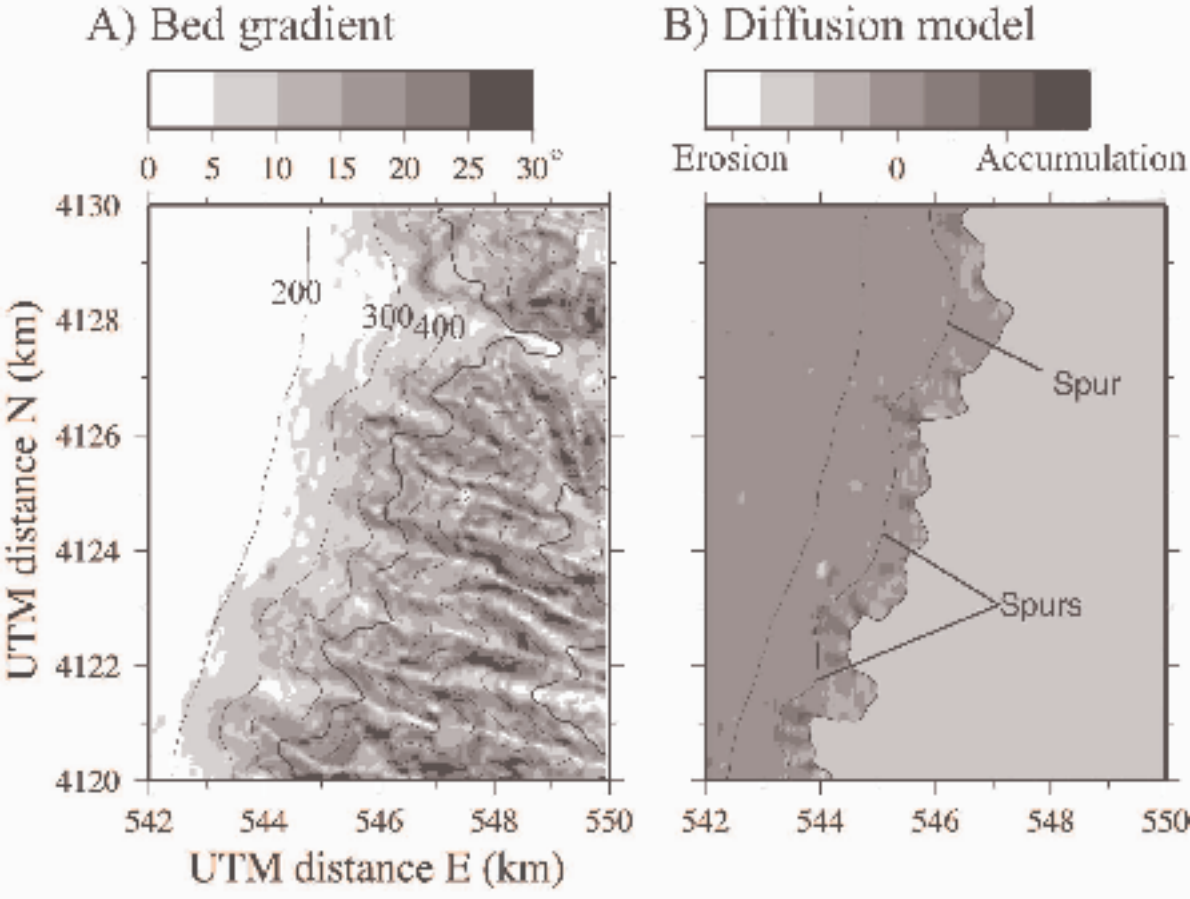
A) Bed gradient
0 5 10 15 20 25 30°
200
300
400
4130
4128
4126
4124
4122
4120
UTM distance N (km)
542 544 546 548 550
UTM distance E (km)
B) Diffusion model
Erosion 0 Accumulation
Spur
Spurs
542 544 546 548 550

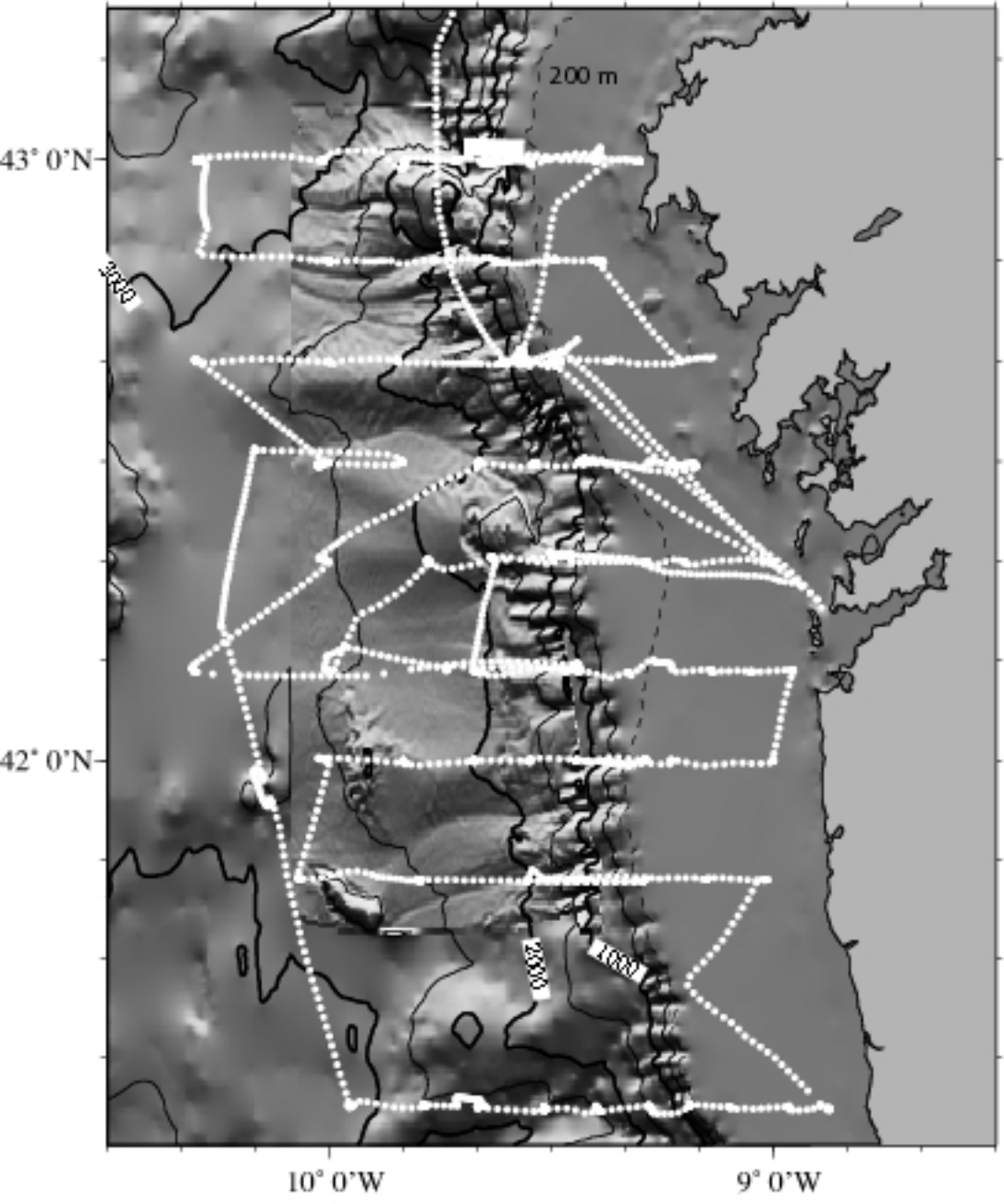
200 m
43° 0'N
42° 0'N
10° 0'W
9° 0'W
3000
2000
1000